Thesis title

Electrochemical Properties of Nanoceria

Master's Degree Program in Physical and Chemical Sciences

Atif Ali

Supervisor: Dr. Mikko Salomäki

Department of Materials Chemistry

University of Turku, Finland.

Acknowledgement

I am thankful to the University of Turku Finland, Department of Material's Chemistry, and the members of materials chemistry research group for their support and co-operation during my thesis work. I am grateful to Professor Dr. Carita Kvarnström for accepting me to the master's degree programme for physical and chemical sciences and providing her unconditional support.

I am also thankful to my supervisor Dr. Mikko Salomäki for his continuous guidance throughout the project passionately, his unreserved support and active follow up is greatly appreciated.

I would also like to acknowledge my beloved family and all friends who have given me the courage and support all the way through this journey.

Table Of Content

Abbreviations

CeO_2	Cerium oxide or (Ceria)
RGO	Reduced graphene oxide
GO	Graphene oxide
FCC	Face centred cubic
ORR	Oxygen reduction reaction
OER	Oxygen evolution reaction
4-NP	*para*-nitro phenol
DMFCs	Direct methanol fuel cells
PEMFC	Proton electron membrane cells
SOFCs	Solid oxide fuel cells
CV	Cyclic voltammetry
RRDE	Rotating ring disk electrode
GC	Glassy carbon
Pt	Platinum
Au	Gold

Abstract

The purpose of the study was to synthesize and examine the electrochemical properties of ceria (CeO_2) nanoparticles and ceria-reduced graphene oxide (CeO_2-RGO) nanocomposites. The synthesis of ceria nanoparticles and ceria-reduced graphene oxide (CeO_2-RGO) nanocomposites were successfully carried out by using hydroxide mediated and sonochemical methods, respectively. The formation of ceria nanoparticles and ceria-reduced graphene oxide (CeO_2-RGO) nanocomposites were confirmed by using characterization techniques such as UV-visible spectroscopy, Fourier-transform infrared (FTIR) spectroscopy, Raman spectroscopy and X-ray diffraction (XRD) techniques. The electrocatalytic reduction of oxygen, super capacitive behaviour of nanoceria and electrocatalytic oxidation of methanol by using nanoceria with cyclic voltammetry (CV) and rotating ring disc electrode (RRDE) techniques were analysed. The high oxidation peak current was observed with ceria nanoparticles coated on glassy carbon (GC) electrode in the electrooxidation of methanol in alkaline media. The electrocatalytic reduction of oxygen was successfully carried out with ceria-reduced graphene oxide (CeO_2-RGO) nanocomposites coated on the glassy carbon (GC) and gold (Au) electrodes. The electrochemical reduction of *para*-nitrophenol was successfully done by ceria nanoparticles coated on glassy carbon (GC) electrode in aqueous solution. The ceria-reduced graphene oxide (CeO_2-RGO) nanocomposites can enhance the electrocatalytic activity by inducing the synergistic effect. It can also have a great impact on the utilization of ceria-reduced graphene oxide (CeO_2-RGO) nanocomposites in the electrochemical devices.

1.Introduction:

1.1 Cerium Oxide (CeO_2):

Cerium is a rare earth metal and member of the lanthanide group. Its atomic number is 58 [1]. It shows catalytic properties because of the shielding effect of 5p and 4d electrons on the 4f orbital [2]. CeO_2 is known as the highly stable oxide of cerium. According to the series of lanthanides, cerium is very reactive element, and it is the second member in it. Cerium is electropositive nature wise. It has two oxidation states such as Ce^{3+} and Ce^{4+}. The oxidation state of Ce^{4+} is more stable as compared to Ce^{3+} because of the electronic structure. The electronic structure of Ce^{4+} is $[Xe]4f^0$, as it is empty, so this is more stable than Ce^{3+} having $[Xe]4f^1$. The two oxides of cerium are CeO_2 (cerium dioxide) and Ce_2O_3 (cerium sesquioxide). As CeO_2 has high stability, so it is used as cerium oxide over Ce_2O_3 [3].

The ceria-based nanostructures are considered very important because of their physico-chemical properties. Pure/doped CeO_2 materials exhibit exceptional catalytic activity and improved oxygen storage capacity. The CeO_2 nanospheres can be doped with various elements for examples samarium (Sm), copper (Cu), carbon (C), cobalt (Co), nitrogen (N), manganese (Mn), sulphur (S), gadolinium (Gd), yttrium (Y), nickel (Ni), phosphorous (P), lanthanum (La) etc. The different methods for the synthesis of ceria-based materials are sonochemical synthesis, sol-gel process, thermal decomposition, homogeneous precipitation etc. Ceria nanostructures are used widely in different fields due to their enormous characteristics [4].

CeO_2 is a significant rare earth material. It has been used in many commercial and technological applications such as catalytic converters, solid oxide fuel cells, diesel oxidation catalysts, sensors, mechanical and chemical polisher, and planarization. It can be used potentially in future also for example treating specific diseases as a therapeutic agent, thermolytic and photolytic water splitting for producing hydrogen and chemical looping combustion [5].

Ceria has many applications because of its potential to store and release oxygen through producing oxygen vacancies as cerium ions such as Ce^{3+} and Ce^{4+} have simply accessible oxidation states. As the interface events and surface are essential for the CeO_2 functionality so, the importance of surface structure and its composition should be well defined and studied [6]. Cerium oxide can consist of +3 and +4 state in the bulk form which supports to become CeO_2 and CeO_{2-x} and then shows antioxidant properties [7]. The catalytic performance is enhanced when the ceria size is decreased to nanometre scale because of increase in the oxygen storage capacity and the enhanced surface area [8].

1.2 Structure of Ceria (CeO_2):

CeO_2 consists of fluorite structure along with a space group of Fm3m. Figure 1 shows the structure of cerium which comprises of cubic oxygen sub-lattice, including the cerium ions having alternative cube centres. It demonstrates the composition of stoichiometric CeO_2, consisting of 8 coordinated cerium (small purple balls) and 4 coordinated oxygen (big red balls). The oxygen atoms are at the corners of the tetrahedron with cerium at the centre [9].

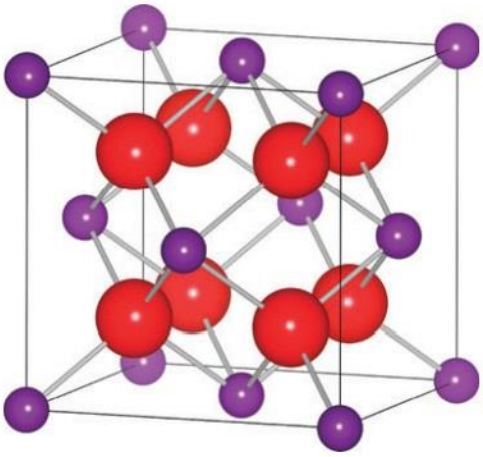

Figure 1. The Ceria FCC structure [9].

1.3 Significance of oxygen vacancies in ceria:

The formation of oxygen vacancies in ceria creates reactive sites and enabling the ionic diffusion which favours its application in solid fuel cells and catalysis [10]. Usually, there are three low index lattice planes on the CeO_2 nanocrystals surface such as (100), (110) and (111). The very famous shape is the (200) and (111) fenced truncated octahedral. The CeO_2 unit cell is composed of fcc (face centred cubic) shaped Ce lattice, and an oxygen of cubic cage shape situated in the face centred cubic cation lattice. The structural model planes of (100), (110), and (111) shows the atoms surface density of the subsequent planes with $n(111) > n(200) > n(110)$. The surface energy of the face centred cubic metal three lowest index planes is $\gamma[111] < \gamma[200] < \gamma[110]$ [11].

The oxygen vacancies on the (110) and (100) planes are more as compared to (111) because on the (111) exposed facet, the formation of energy of oxygen vacancies is greater than (110) and (100) facets. Such as generally shape of nanoparticles are octahedral or truncated

octahedral, so they are mostly subjected to highly stable (111) facets for maintaining the surface energy at least possible. Whereas one dimensional nanostructures (nanowires and nanorods) have (110) and (100) planes because three-dimensional nano cubes can show (100) planes. So, more oxygen vacancies are present on the surfaces of nanorods and nano cubes. Many other external or internal aspects like doping elements and temperature can be influenced by the concentration of oxygen vacancies present in the crystal [3,12]. The presence of oxygen vacancies and their movement in crystal is very crucial. The oxygen atoms can move easily within the crystal when the oxygen vacancies are at high concentration, this facilitates the redox reaction on the surface for exceptional catalytic performance [3].

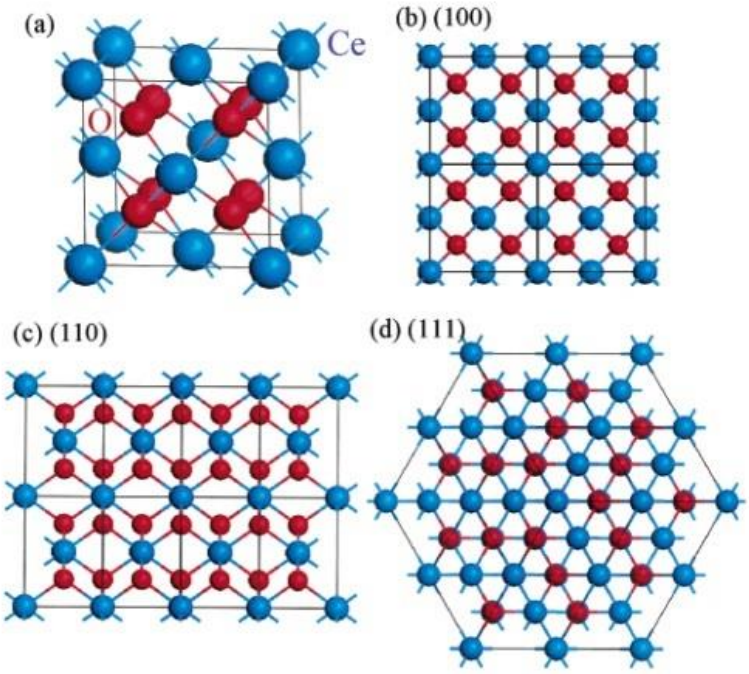

Figure 2. (a) CeO_2 structure (unit cell). (b-d) The CeO_2 structure planes (100 or 200), (110), and (111) [11].

Jing L. et al. synthesized porous nanorods of ceria by hydrothermal method. The porous nanorods of ceria shows improved capacity to store oxygen and its reducibility. This leads the surface area to enlarged and the defects in further types of nanoceria. The porous nanorods of ceria performs enhanced catalytic activity. In this way they proved to promote the catalytic activity in the oxidative processes. The oxygen vacancy development becomes noticeable when the crystals of CeO_2 decreases to the size of nanoscale. The existence of structural defects is

also associated as primary oxygen vacancies. It can control or improve the surface chemistry of nanostructure of ceria (nanoceria). Adding the adjustable redox couple of Ce^{3+}/Ce^{4+}, the multifunctional performance exhibits the surface of CeO_2. The nanostructure of CeO_2 can produce various useful applications in catalysis due to its multi-functionalized surface properties. The catalytic behaviour of CeO_2 catalysts is affected by how the reduction of CeO_2 surface is done and how to store the oxygen. Hence the performance depends on the efficiency of material frequently moving through the redox cycles of Ce^{3+}/Ce^{4+} [13].

Hailstone R. K. et al. synthesized CeO_2 nanoparticles which were colloidally stable by using method of aqueous precipitation. The nano-sized particles are very important to develop for finding the particle reactivity because when the size of particle is decreased, there is expansion in the lattice of nanoceria which decreases its ability of reabsorption and oxygen release. The electron diffraction analysis proves that the smallest size CeO_2 nanoparticles up to 1.1 nm was having persistent structure with fluorite lattice. The particles consist of significant quantities of Ce^{3+} at this size. This linked collectively with the oxygen vacancies to form enhanced lattice expansion and lattice strain. The results of the previous studies proves that ceria nanoparticles of ultra-small size of 1.1 nm, significant percentage of the atoms of ceria holds the reduced state, although the ceria nanoparticles have lattice of cubic shape instead of hexagonal shape [14]. Deshpande et al. also proposed the relation among the lattice parameter and the size of particle in the particles of nano cerium oxide having size of (3-30 nm). The change in the lattice parameter is linked to the lattice strain caused by the Ce^{3+} and developing oxygen vacancies. As the particle size increases, the lattice strain decreases and as the particle size reduces, the concentration of Ce^{3+} increases [15].

2. Graphene and reduced Graphene Oxide (RGO):

The pristine graphene is made up of sp^2 hybridized carbon sheets. They are free of the defects. They are not produced in mass quantities, so they are rarely used in electrochemistry as an electrode material. That is why graphene generated from graphite by chemically modifying are utilized [16]. Graphene oxide (GO) is derived from graphene along with the functional groups for example hydroxyl, epoxy and carboxylic acid groups connected to it [17].

Graphene oxide (GO) can be reduced to make reduced graphene oxide (RGO) by techniques such as thermal, chemical, or electrochemical processes. There are two significant characteristics of GO. First, it can be produced as a raw material from low-cost graphite through

inexpensive chemical methods for high production. Second, it can be used for to form aqueous colloids to enable the gathering of macroscopic structures through facile solution processes. Both the characteristics are valuable because of the practice of graphene at large scale [18].

RGO, reduced graphene oxide, is a chemical functional atomic thin carbon sheet and it gives an easy path for producing low cost, large scale, and high yield production of graphene by solution processing [19].

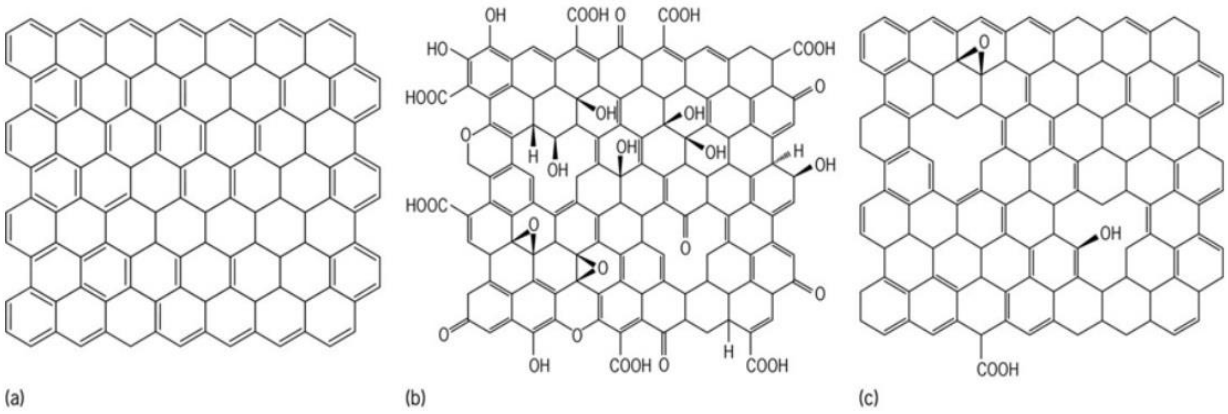

Figure 3. The structures of a) Graphene b) Graphene oxide and c) reduced Graphene oxide (RGO) [20].

The nanocomposites of CeO_2-RGO indicates amazingly improved catalytic performance because of the synergistic effects among the nano ceria and RGO as compared to the bare nano ceria [21]. On the surface of the nanoparticles of ceria, the oxygen vacancies produce localized electrons, they can also enhance the properties of RGO by interacting with the functional groups in the reduce graphene oxide sheets [19,22]. The metal oxides for example ZnO, Co_3O_4, TiO_2 and RuO_2 formed nanocomposites with reduced graphene oxide (RGO) have unique properties and are used in different applications [23-26].

Dezfuli A.S. et al. have used an easy and effective sonochemical method for the synthesis of ceria (CeO_2) and ceria reduce graphene oxide (CeO_2-RGO) nanocomposites. They have also examined the CeO_2-RGO nanocomposites for their electrochemical properties. They exhibit a synergistic effect. Moreover, nanocomposites catalytic performance was calculated along with their uses in biomolecules ascorbic acid (AA), uric acid (UA) and dopamine (DA) [22].

3. Oxygen reduction reaction (ORR) and oxygen evolution reaction (OER):

The oxygen evolution reaction (OER) and oxygen reduction reaction (ORR) are the main electrode processes used for the energy methods like recreative fuel cells and the rechargeable metal-air batteries [27]. The oxygen is the richest element of earth crust. The oxygen reduction reaction (ORR) plays a crucial role in the process of life for example biological respiration and in fuel cells as energy conversion procedures. The oxygen reduction reaction (ORR) in acidic aqueous solutions proceeds by a direct 4-electron reduction pathway ($O_2 + 4H^+ + 4e^- \rightarrow H_2O$) and the indirect 2-electron reduction pathway ($O_2 + 2H^+ + 2e^- \rightarrow H_2O_2$) and H_2O_2 further reduce to water ($H_2O_2 + 2H^+ + 2e^- \rightarrow 2H_2O$). Whereas in alkaline aqueous solutions, the oxygen reduction reaction (ORR) proceeds by a direct 4-electron pathway ($O_2 + 2H_2O + 4e^- \rightarrow 4OH^-$) and the 2-electron pathway ($O_2 + H_2O + 2e^- \rightarrow HO_2^- + OH^-$) and HO_2^- ions further reduce to $3OH^-$ ($HO_2^- + H_2O + 2e^- \rightarrow 3OH^-$). The reduction pathway of 1-electron can take place from O_2 to O^{2-} (superoxide) in the (non-aqueous) aprotic solvents ($O_2 + e^- \rightarrow O_2^-$). The direct 4-electron reduction pathway is favoured in the fuel cell process. The H_2O_2 is produced industrially by the indirect 2-electron reduction pathway. Whereas the reduction pathway of 1-electron is crucial for ORR mechanism [28]. The platinum can be used as a common reference for oxygen reduction reaction (ORR) because it shows higher catalytic activity, but it has limited practical applications because of inadequate capability of anti-methanol poisoning, expensive and barely slight activity for oxygen evolution reaction (OER). On the other hand, metal oxides can be a good substitute because it is efficient and cost-effective bifunctional catalysts for oxygen reduction reaction (ORR) and oxygen evolution reaction (OER). The drawbacks of these catalysts such as weak stability, low conductivity and small surface area limited their applications [27]. Sun L. et al. stated that composite of CeO_2-RGO can be produced at room temperature from sonochemical method. They examined the material prepared to be used as the bifunctional catalyst for OER and ORR. In alkaline media, it exhibits the outstanding catalytic performance and stability for OER and ORR. The catalytic activity of high oxygen reaction provides the synergistic effect to the fast transport of electron of reduce graphene oxide and high electrocatalytic performance of ceria. [27].

Bag S. et al. established a method for the synthesis of electrocatalyst based on N-doped reduced graphene oxide (N-RGO) and transition metal oxide along with the enhanced electrocatalytic performance for oxygen reduction reaction (ORR) in the alkaline media. Transition metal oxide embedded with N-doped carbon systems similarly encourages the catalytic activity of oxygen reduction reaction (ORR) by enabling the transfer of electron [29].

4. Direct methanol fuel cells (DMFCs):

Methanol can be obtained commercially from the synthesis gas [30]. Methanol is used in the application of fuel cell as a favourable hydrogen (H_2) source [31]. Direct methanol fuel Cells are best applicant for application in laptop computers, cell phones and other digital compact devices. DMFC are suitable because of their cost effectives, good electronic performance, efficient and they do not need any pressurized H_2 gas. The reduction of O_2 to H_2O efficiently is important task in energy conversion in Direct Methanol Fuel Cells (DMFCs). In alkaline DMFCs, the oxygen reduction reaction (ORR) proceeds by a 4-electron pathway ($O_2 + 2H_2O + 4e^- \rightarrow 4OH^-$) and it is better than the 2-electron pathway ($O_2 + H_2O + 2e^- \rightarrow HO_2^- + OH^-$) [28,32].

Kaur B. et al. prepared the cerium oxide (CeO_2) decorated with nanocrystalline zeolite nanocomposites by calcination of nanocrystalline CeO_2 and zeolites at various weight ratios. The material used in the methanol oxidation were examined as valuable metal-free electrode catalyst. The methanol electrochemical oxidation was examined by CeO_2/zeolites with improved glassy-carbon electrode in alkaline solution. The 30% weight ratio of CeO_2/zeolites shows high catalytic performance in the oxidation of methanol as compared to the nanocrystalline CeO_2 and industrially used catalyst of Pt (20%)/C. The enhanced electrocatalytic performance in the oxidation of methanol is because of the synergistic effect of nanocrystals of CeO_2 and the enhanced surface area of nanocrystalline zeolites. Their findings suggest that as CeO_2/zeolites has high stability and current density, so it is commercially useful in the applications in DMFCs [33].

Salarizadeh P. et al. used hydrothermal method to synthesize CeO_2 and CeO_2-RGO. These nanoparticles are used in the oxidation of methanol initially. The CeO_2-RGO nanocomposites shows increased electrocatalytic performance and improved stability for the oxidation of methanol in alkaline solution. The CeO_2-RGO composite possesses low resistance for charge transfer, enhanced surface area and disperse CeO_2 steadily on RGO. So, it can be used in application in supercapacitors, lithium-ion batteries, and various reactions of electro-oxidation [34].

5. Proton exchange membrane fuel cells (PEMFC):

Recently the PEM fuel cells are of great interest because they possess high energy density, low emissions and highly efficient. They are used in different applications of stationary, transportation, micro power, and portable power. The Pt-based nanoparticles are the most useful catalysts in PEM fuel cells. Though there are various disadvantages of Pt-based catalysts for example they are expensive, no acceptance for methanol oxidation, contaminant sensitive and less fulfilled 4 electron reduction reaction [28].

PEM fuel cells can be utilized in the practical applications by increasing the performance of cell and reducing the cell fabrication cost. The performance of PEM fuel cells is dependent on the oxygen reduction kinetics associated with the cathode half-cell reaction [35,36]. So more nonprecious metal oxide electrocatalysts are focused to develop efficiently for ORR. As CeO_2 and doped CeO_2 have unique structural properties among the numerous rare earth metal oxides, so they possess good electrocatalytic activity. The Ce^{4+} ion is likely to reduce into Ce^{3+} ion, which leads to an electronic conductivity of mixed ion in the nanostructure of CeO_2 [35,37].

Parwaiz S. et al, used simple hydrothermal method for the synthesis of (cobalt) Co-doped CeO_2/RGO nanocomposites. The Co-doped CeO_2 nanoparticles having a diameter of 4-7 nm were attached steadily on the sheets of RGO, which results in the formation of composite that shows improved performance of supercapacitor and increase in ORR activity. The improved 3% Co-doping presents increased ORR activity and energy storage performance compared to other composites. The enhanced performance with 3% Co-CeO_2/RGO is associated with the synergistic effect of Co-doping, it produces the defects for further active sites whereas RGO improves the adsorption of oxygen (O_2) and the electronic conductivity. The Co-doped Co-CeO_2/RGO shows improved methanol tolerance performance and are more stable when contrasted with the Pt/ C, they are extremely suitable for the ORR catalyst to utilize in DMFCs. The study on 3% Co-CeO_2/RGO nanocomposites is considered to be important because of its contribution towards conversion system and energy storage due to inexpensiveness and ability to synthesis simply [35].

6. Solid oxide fuel cells (SOFCs):

Since last few years, modern energy transformation and storage technologies requires to grow more because of the increasing demand for energy and environmental degeneration. Solid oxide fuel cells transform the fuels chemical energy to electrical energy effectively and without environmental problems. The benefits of SOFCs are multi fuel choice and the kinetics of fast

electrode because of elevated operational temperature. But high operating temperature restricts their use commercially. So, to decrease the working temperature, efforts were done to produce solid electrolytes displaying high conductivity at low temperature. Ceria solid electrolytes indicates high conductivity at 500-700°C. Further the nanocomposites or doped/co-doped ceria produced in alkali salts decreases the operating temperature. There are three elements of SOFCs such as cathode, anode, and electrolyte [38].

The energy conversion method of fuel cells involves the fuel electro oxidation at anode. Previously it proved that when the (ceria) CeO_2-based oxides is present in SOFCs anodes including the electrolytes conducting oxygen ion then the activation overpotential of the oxidation of hydrogen decreases. Mostly porous and electrode composite structures having unrestrained interfacial properties and poorly defined geometry were used in those studies. Whereas now the ceria metal structures with controlled interfacial properties and well-defined geometry were used. The nano structuring of ceria as pathway to improve activity instead of the conventional concept of nano structuring of metal catalyst [39].

7. Supercapacitors:

The electrochemical supercapacitors are known as the most essential invention between all the conversion and energy storage technologies. The electrochemical supercapacitors are also identified as ultracapacitors, supercapacitors and electrochemical double layer capacitor. This type of capacitor has more capacity to store energy density as compared to the storage capacity of other traditional capacitors. The electrochemical supercapacitors have properties that highly impact its value for example they have ability of fast charging, broadly operatable at temperature ranges and long charge discharge cycle. They have wide applications in electrical developments. There are few challenges in their application such as expensive and comparatively low energy density so further studies are required to make it suitable to work with fuel cells and batteries and operate as solo high energy storage tools [40].

The nano ceria is a good redox supercapacitor material because ceria contains exceptional redox characteristics and it is environmentally friendly, cost effective and rich rare earth metal oxide. The nanostructure of ceria with improved surface area effects the pseudo capacitance. Dezfuli A.S. et al. used sonochemical method for synthesizing nanocomposite material of ceria (CeO_2) and reduced graphene oxide (RGO) for the application in supercapacitors. The nanoparticles of CeO_2 are attached on RGO sheets to increase the materials specific capacitances. They have also examined various studies of nanostructure and electrochemical

activities of nano CeO_2 anchored on RGO sheets. The CeO_2-RGO nanocomposite electrodes shows high super capacitive activity along with enhanced specific capacitance of 211 F g^{-1} at 2 mV s^{-1} and 185 F g^{-1} at 2.0 A g^{-1}, easily reversible and highly capable [41].

Deng D. et al. used cost effective and simple chemical co-precipitation process to synthesis nanostructured CeO_2 nanoparticle-decorated GO. The size of ceria nanoparticle in nanoceria decorated GO with ratio 1:4 sample was approximately 2-3 nm. The electrochemical examination shows that sample electrode obtains high specific capacitance of 382.94 F g^{-1} with the current density of 3.0 A g^{-1} [42].

Li and co-workers used an in-situ method for the synthesis of ceria graphene nanocomposite, indicating the specific capacitance of 208 Fg^{-1} and highest power density 18 kW kg^{-1} in the supercapacitors [43].

8. Reduction of CO_2:

The use of CO_2 through electrochemical reduction to produce fuels or chemicals by utilizing the alternating sources of energy resources. So, the molecular electrocatalysts are constantly examined and modern developments in the catalytic properties and mechanistic awareness are appreciable. Previously, complexes of rare metal centres are focused to examine such as ruthenium (Ru), rhenium (Re), and palladium (Pd). But recently, the focus of the study has been moved towards transition metals abundantly found in earth for example cobalt (Co), manganese (Mn), nickel (Ni), and iron (Fe) [44].

Esrafilzadeh D. et al. produced liquid metal electrocatalyst that comprises of metallic elemental nanoparticles of cerium. So, at very low potential of -1.2V vs Ag/Ag^+, -310 mV vs CO_2/C, this helps to establish electrochemical reduction of CO_2 to layered solid carbonaceous species. The reduction of CO_2 at room temperature was supported by using the cerium oxide catalyst at liquid metal or electrolyte interface and cerium nanoparticles. At Liquid metal electrode, the Ce^{3+} is reduced to Ce^0 at low potential**.** The pathway of catalysis was known due to get approach to Ce^0. So, at the liquid interface, the inhibition shown by van der Waals adhesion leads the electrode to extremely show resistance towards deactivation through coking that occurs because of solid carbonaceous species. The solid carbonaceous materials can be used in manufacture of capacitor electrodes. So, the liquid metal facilitates the electrocatalytic process at room temperature to possible work in a negative emission technology. Further at high potential CO is formed which is used as precursor for making synthetic fuels and chemicals

industrially. The electrochemical reduction of CO_2 was carried out by utilizing the LMCe catalysts. The real LM (control) was performed in dimethylformamide (DMF)-based electrolyte because CO_2 is highly soluble in the solvent. LSV (Linear sweep voltammetry) was performed by using saturated electrolytes of CO_2 or N_2 (control). In the existence of CO_2, the cerium alloys help the current densities and presented low potentials of -310 mV vs. CO_2/C). A substantial current density was seen when the electrochemical examinations were done in saturated electrolytes of CO_2. This indicates that the electrochemical methods are carried out in the existence of CO_2 dissolved [45].

9. Photocatalysis:

The photocatalytic systems are in great demand to be developed for the water splitting as they can be used in the formation of solar fuels [46]. Primo A. et al. reported the catalytic activity of nanoceria for the formation of oxygen form water. The size of the particles of ceria effects the photocatalytic performance. Further, the nanoparticles of gold were deposited at low loading to enhance the photocatalytic performance for samples producing visible light. This indicated the improved photocatalytic activity as compared to the similar material when irradiated with bandgap. The samples of ceria comprising gold in visible light irradiation serves as the WO_3 photocatalytic activity in UV irradiation. This study leads the ceria to be used as photocatalyst for furthermore reactions [47].

Verma R. et al. used facile hydrothermal reactions to synthesize in situ CeO_2 grafted graphene. In this reaction ceria concentration is altered instead of graphene. The hydrothermal method assisted by ammonia is used to produce (CeO_2-RGO) nanocomposites without using toxic reducing reagent. The improved photoactivity of the catalyst is accountable of increased photo sorption, elevated dye absorptivity and greater charge separation and attributes of transportation. The CeO_2 and graphene interface plays crucial role for photocatalytic elimination of methyl orange, and it is analysed by taking numerous samples of different quantities of ceria. Later it shows increased performance of photodegradation of methyl orange in the clear light irradiance. In the composite, the CeO_2 concentration in RGO regulates the photoactivity. So, the composite of CeO_2 in RGO with ratio of 2:1 shows increased photoactivity than bare CeO_2 catalyst. Their results support the importance of graphene-CeO_2 interface in charge separation and the content of CeO_2 [48]. Ji Z. et al. synthesized CeO_2-reduced graphene oxide (RGO) nanocomposites by using two techniques named as in situ and self-assembly. They proposed that CeO_2-reduced graphene oxide (RGO) nanocomposites

proved the improved photocatalytic activity for the degradation of methylene blue below the irradiation of simulated sunlight as compared to the CeO_2 nanoparticles [49].

Para-nitrophenol (PNP) is a poisonous compound and during the production and processing of various industrial goods, it can contaminate the environment. The *p*-nitrophenol (PNP) electrocatalytic reduction towards *p*-hydroxyl aminophenol in aqueous media by utilizing the electrode of metallic gold has been reported. The *p*-hydroxyl aminophenol was employed as standard material to examine the catalytic performance of the metal gold electrode. [50].

Miah A. T. et al. reported the catalytic activity stimulated by solar light for *p*-nitrophenol reduction through CeO_2 and nano gold (Au) catalyst driven over CeO_2 and CeO_2-TiO_2 with molar ratio (1:1). The photocatalytic reduction of 4-NP (*p*-nitrophenol) on Au/CeO_2-TiO_2 catalyst. The Au/CeO_2-TiO_2 catalyst was used for catalytic reduction caused by solar light because 4-NP reduction caused by natural sunlight is a sustainable process. So, they have examined the CeO_2, and gold deposited ceria catalysts for initiating 4-NP (*p*-nitrophenol) reduction below the solar light by applying the reducing agent as $NaBH_4$ [51].

The clear cathodic peak exhibit by the para-nitrophenol and ortho-nitrophenol at around -0.83 V and -0.72 V, that are linked with the nitryl irreversible reduction process in the aqueous media [52].

10. Experimental Part

10.1 Materials and methods:

10.1.1 Synthesis of CeO_2 Nanoparticles:

The simple hydroxide mediated method was used to synthesize CeO_2 nanoparticles [53]. The cerium nitrate hexahydrate and sodium hydroxide were used as the precursor for the synthesis of CeO_2 nanoparticles by hydroxide mediated method. We prepared 0.1M cerium nitrate hexahydrate $Ce(NO_3)_3.6H_2O$ (50 ml) and 0.3M sodium hydroxide (NaOH) (20ml) solution in distilled H_2O. The sodium hydroxide (NaOH) solution was added dropwise to the cerium nitrate hexahydrate $Ce(NO_3)_3.6H_2O$ solution under constant magnetic stirring for around 2 hours at room temperature. After that we got precipitate of pinkish white color and then centrifuged it at 2000 rpm for 15 minutes. The pellet was obtained by discarding the supernatant. Then the pellet was washed several times with distilled water (H_2O) and later with ethanol. The pellet was dried at 80°C for 1 hour in oven and subsequently annealed it at 270°C for 24 hours. The resulting product obtained was CeO_2 nanoparticles of yellowish color.

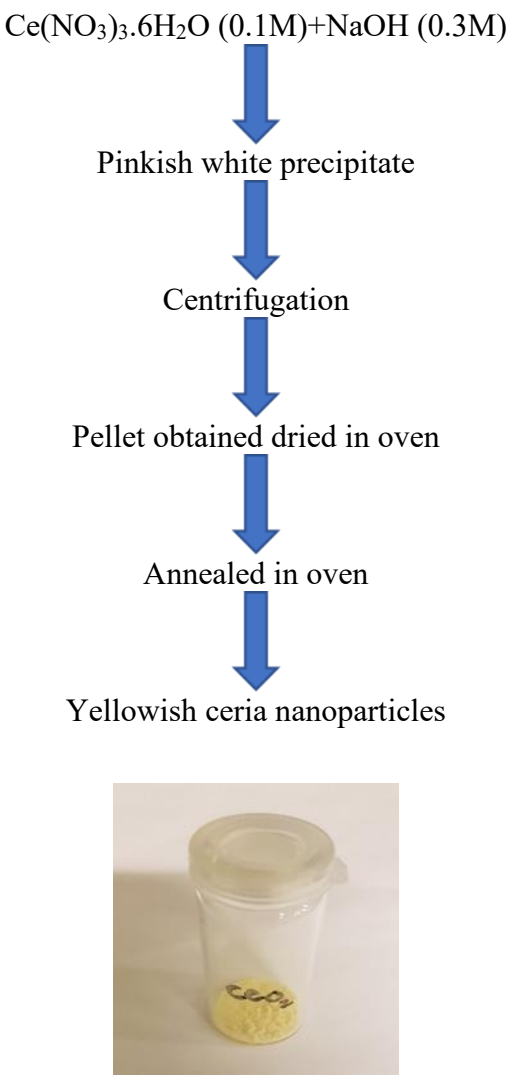

Figure 4. The flow diagram of (CeO_2) nanoparticles synthesis.

10.1.2 Synthesis of (CeO_2-reduced Graphene Oxide) nanocomposites:

The synthesis of the (CeO_2-RGO) nanocomposites was done by a novel sonochemical method [22]. We prepared 0.1M cerium nitrate hexahydrate $Ce(NO_3)_3.6H_2O$ (20ml) solution in distilled water. After that we added 25% ammonium hydroxide (NH_4OH) dropwise in the above solution for approximately 1 hour during ultrasonic irradiation in the ultrasonic bath. Later the suspension of Graphene oxide (GO) (60ml) of concentration (0.5mg/ml) was added to the above suspension with constant magnetic stirring and then sonicated it again for 25 minutes. The mixture obtained was heated at 90°C and after that we added hydrazine (N_2H_4) (3ml) to the mixture and refluxed it for 1 hour. The precipitate obtained was washed several times with

distilled water and ethanol. Then dried it at 60°C for 24 hours. The resulting product obtained was (CeO_2-RGO) nanocomposites.

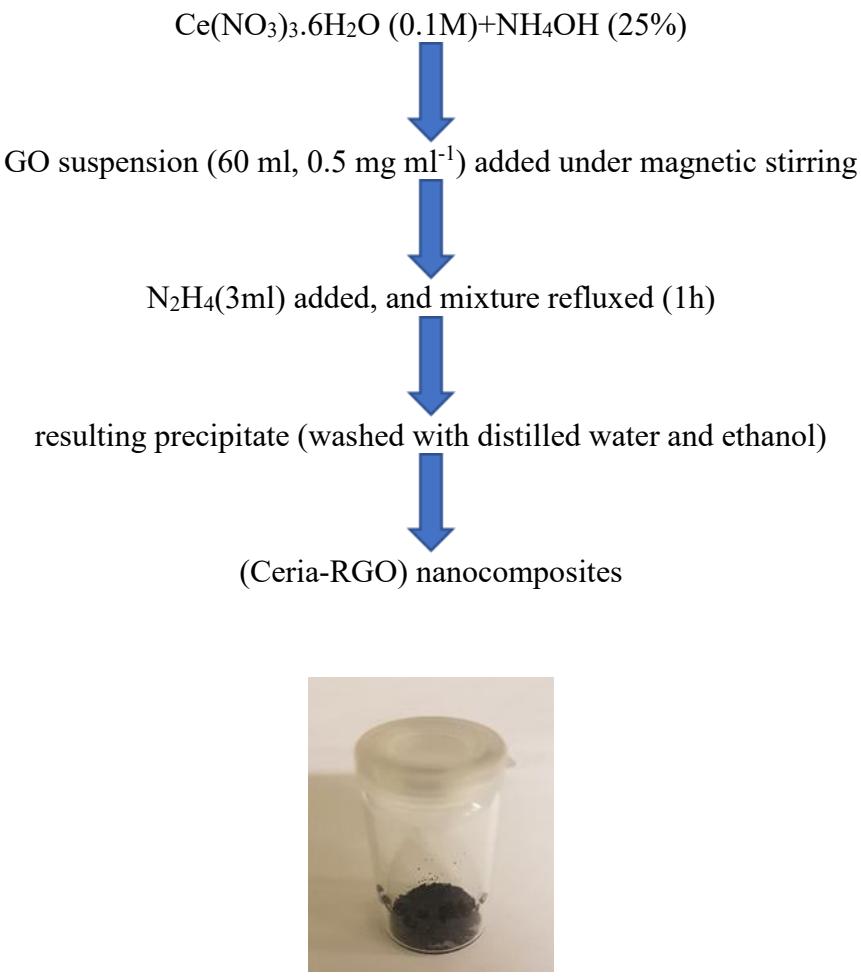

Figure 5. The flow diagram of (CeO_2-RGO) nanocomposites synthesis.

11. Characterization:

The UV-visible spectroscopy was used for the optical studies of CeO_2 nanoparticles. The concentration of Cerium oxide (CeO_2) was used 100 ppm in distilled water and the pH of the solution was (pH=6) and tested the sample with Agilent Cary 60 UV-Visible spectrophotometer. The water was used as a blank. The strong absorbance was observed below 400 nm in UV-visible absorbance spectrum and a well-defined absorption peak at 269 nm confirms the formation of CeO_2 nanoparticles as shown in figure 6 [53,54].

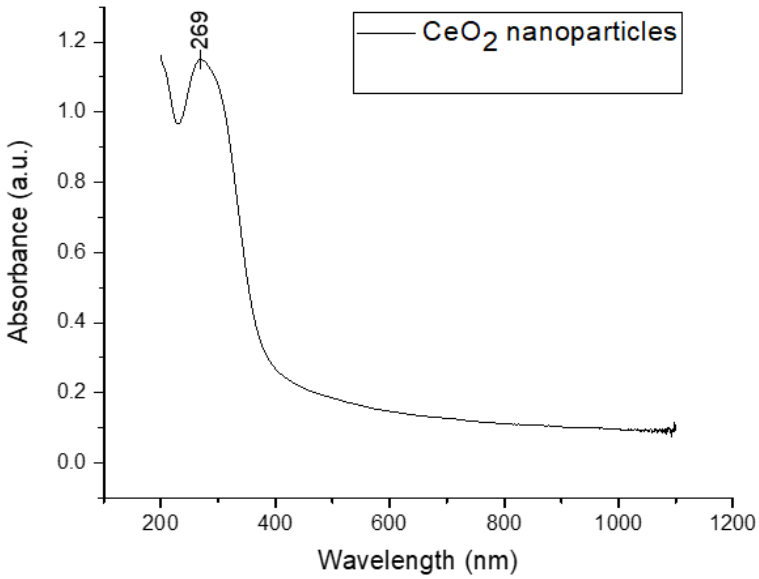

Figure 6. UV-visible absorption spectrum of cerium oxide (CeO_2) nanoparticles.

The UV-visible spectroscopy was used for the optical studies of (CeO_2-RGO) nanocomposites. The concentration of (CeO_2-RGO) nanocomposites was used 100 ppm in distilled water and tested the sample with Agilent Cary 60 UV-Visible spectrophotometer. The water was used as a blank. A strong absorbance was observed below 400 nm in UV-visible absorbance spectrum and a well-defined absorption peak at 296 nm confirms the formation of ceria as shown in figure 7 [54].

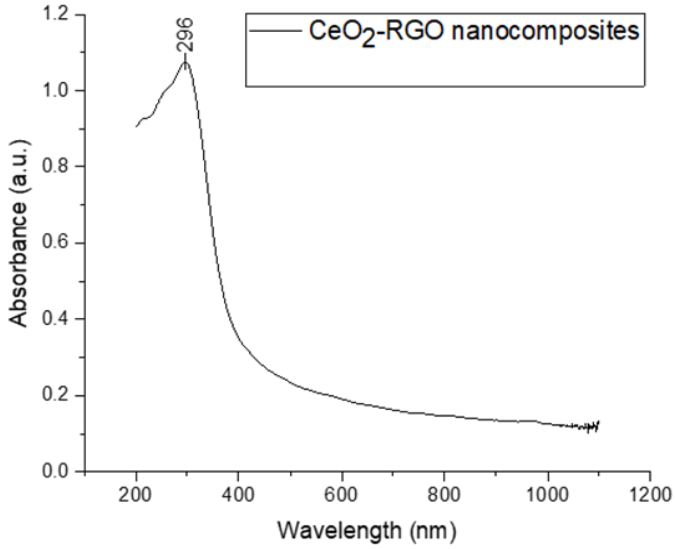

Figure 7. UV-visible absorption spectrum of (CeO_2-RGO) nanocomposites.

The CeO_2 nanoparticles powder was tested with Brucker FTIR instrument. The intensive band at 1321 cm^{-1} corresponds to the N-O stretch. The bands around 1531 cm^{-1} and 3395 cm^{-1} corresponds to water and hydroxyl stretch. The Ce-O stretch showed signal around 500 cm^{-1} as shown in figure 8 [53]. The Ce-O peak is hidden and further confirmed by using Raman spectroscopy. That confirmed the formation of CeO_2 nanoparticles.

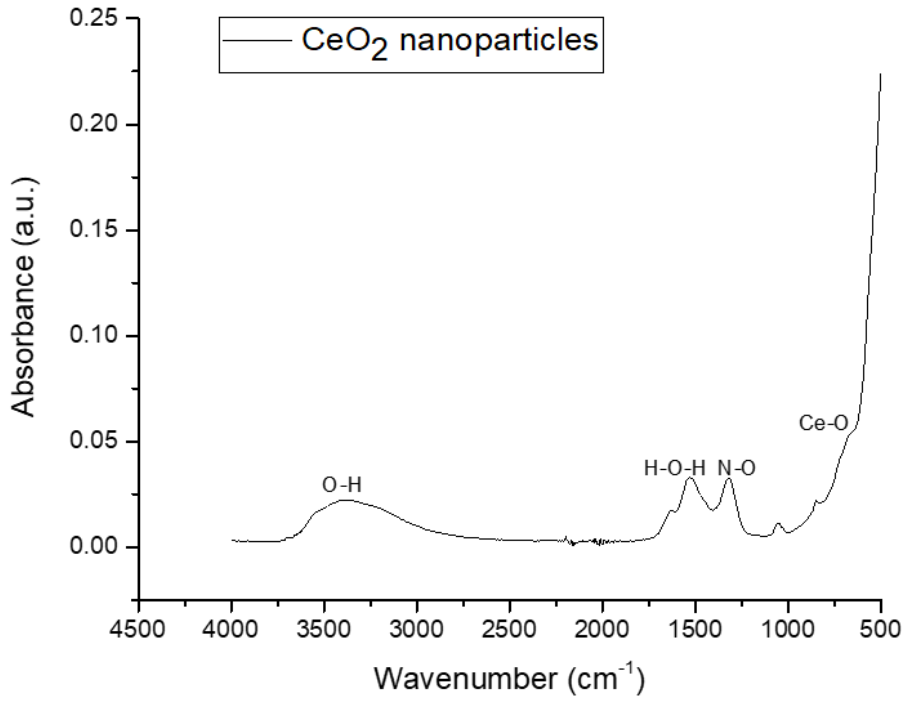

Figure 8. FTIR spectrum of (CeO_2) nanoparticles recorded using diamond ATR crystal.

The (CeO_2-RGO) nanocomposites powder was tested with Brucker FTIR instrument. The FTIR spectrum of (CeO_2-RGO) showed broad band around 3000 cm^{-1} corresponds to hydroxyl stretch. The bands at 1529 cm^{-1} and 1431 cm^{-1} corresponds to the graphene characteristic stretch. The Ce-O stretch showed signal around 500 cm^{-1} as shown in figure 9. The Ce-O peak is hidden and further it is confirmed by using Raman spectroscopy. That confirmed the formation of CeO_2 nanoparticles and RGO and are well anchored [22].

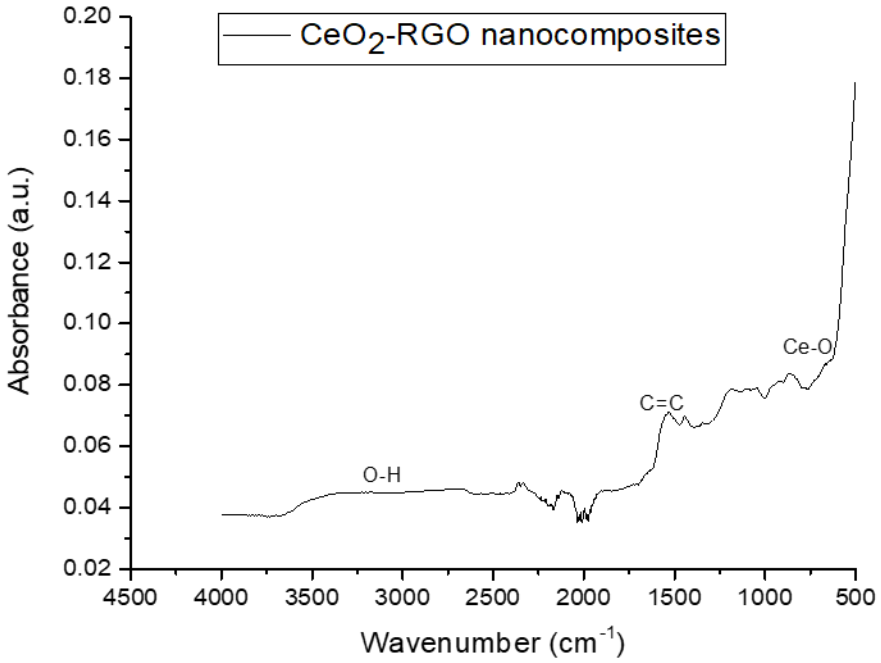

Figure 9. FTIR spectrum of (CeO_2-RGO) nanocomposites recorded using diamond ATR crystal.

The (CeO_2+pyrrole) nanocomposites powder was tested with Brucker FTIR instrument. The FTIR spectrum of (CeO_2+pyrrole) showed broad band around 3000 cm^{-1} corresponds to N-H stretch. The band at 1639 cm^{-1} corresponds to C=O stretch. The bands present at 1527, 1432 and 1041 cm^{-1} correspond to C=C, C-N and C-C out of the plane vibration showed that polypyrrole is formed [56,57]. The Ce-O stretch showed signal around 500 cm^{-1} as shown in figure 10. Which confirmed the formation of (CeO_2+pyrrole) nanocomposites.

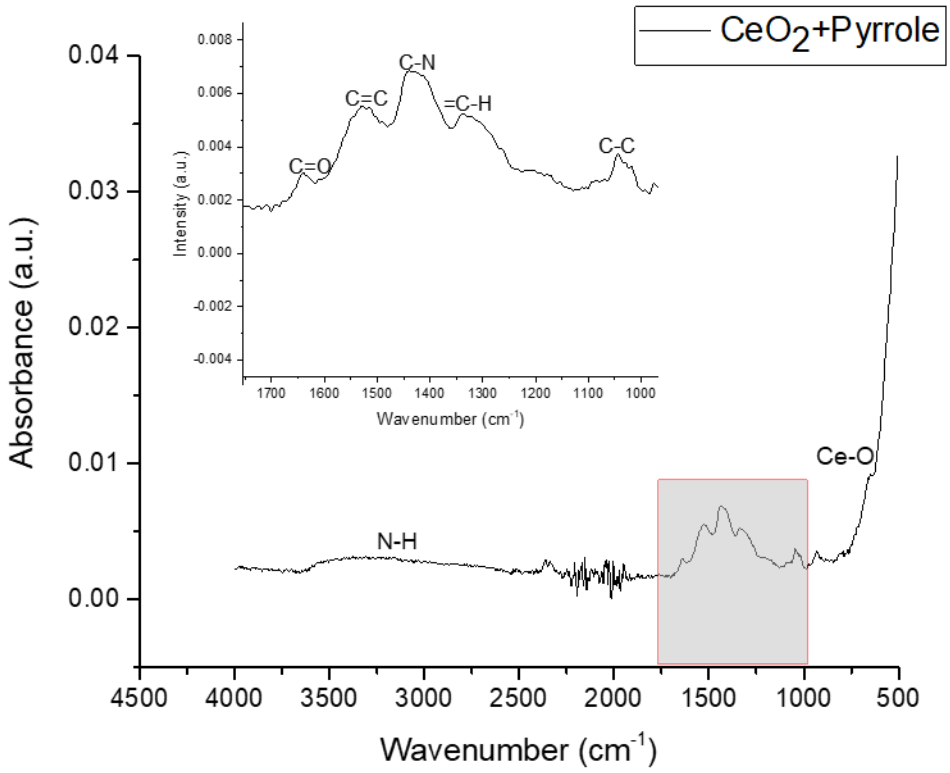

Figure 10. FTIR spectrum of (CeO_2-pyrrole) nanocomposites recorded using diamond ATR crystal.

The Renishaw Qontor inVia Raman microscope instrument was used to test the CeO_2 nanoparticles drop casted on quartz. The Raman spectrum of CeO_2 nanoparticles showed a strong peak at 459 cm^{-1} which corresponds to the symmetrical stretching mode of $Ce\text{-}O_8$ that confirmed the formation of CeO_2 nanoparticles successfully as shown in figure 11 [22].

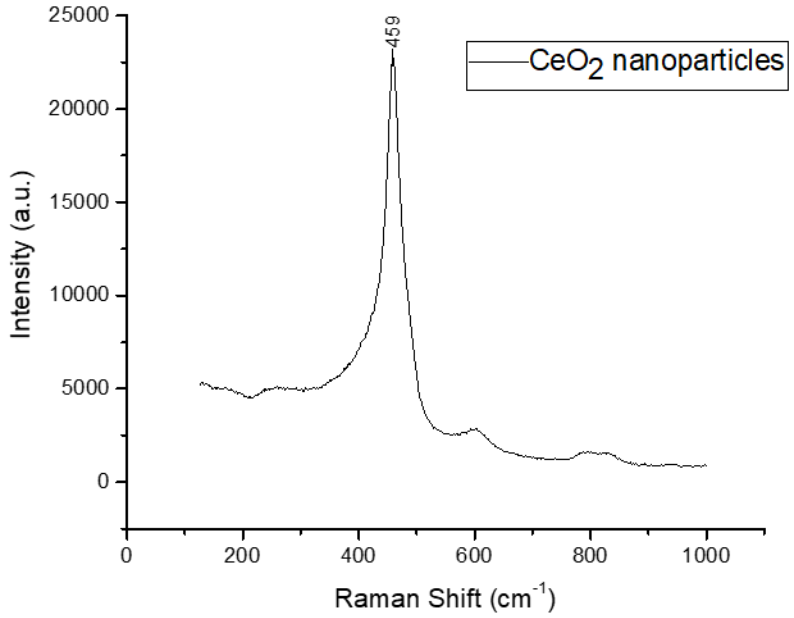

Figure 11. Raman spectrum of (CeO_2) nanoparticles.

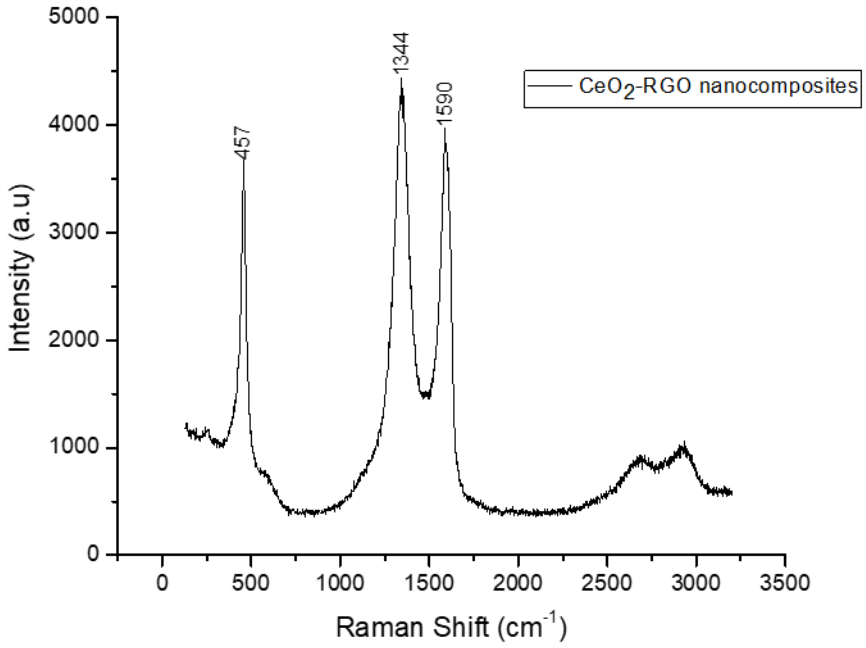

Figure 12. Raman spectrum of (CeO_2-RGO) nanocomposites.

The Renishaw Qontor in Via Raman microscope instrument was used to test the CeO_2-RGO nanocomposites drop casted on the quartz. The Raman spectrum of CeO_2-RGO nanocomposites showed strong peak at 457 cm^{-1} which corresponds to the symmetrical stretching mode of Ce-O_8. The other two strong peaks at 1344 cm^{-1} and 1590 cm^{-1} corresponds to D and G band. The D band is related to the structural defects and G band is linked to the carbon sp^2 atoms (in-plane vibration). This confirmed the formation of CeO_2 nanoparticles and showed that CeO_2 nanoparticles are nicely anchored on reduced graphene oxide (RGO) as shown in figure 12 [22].

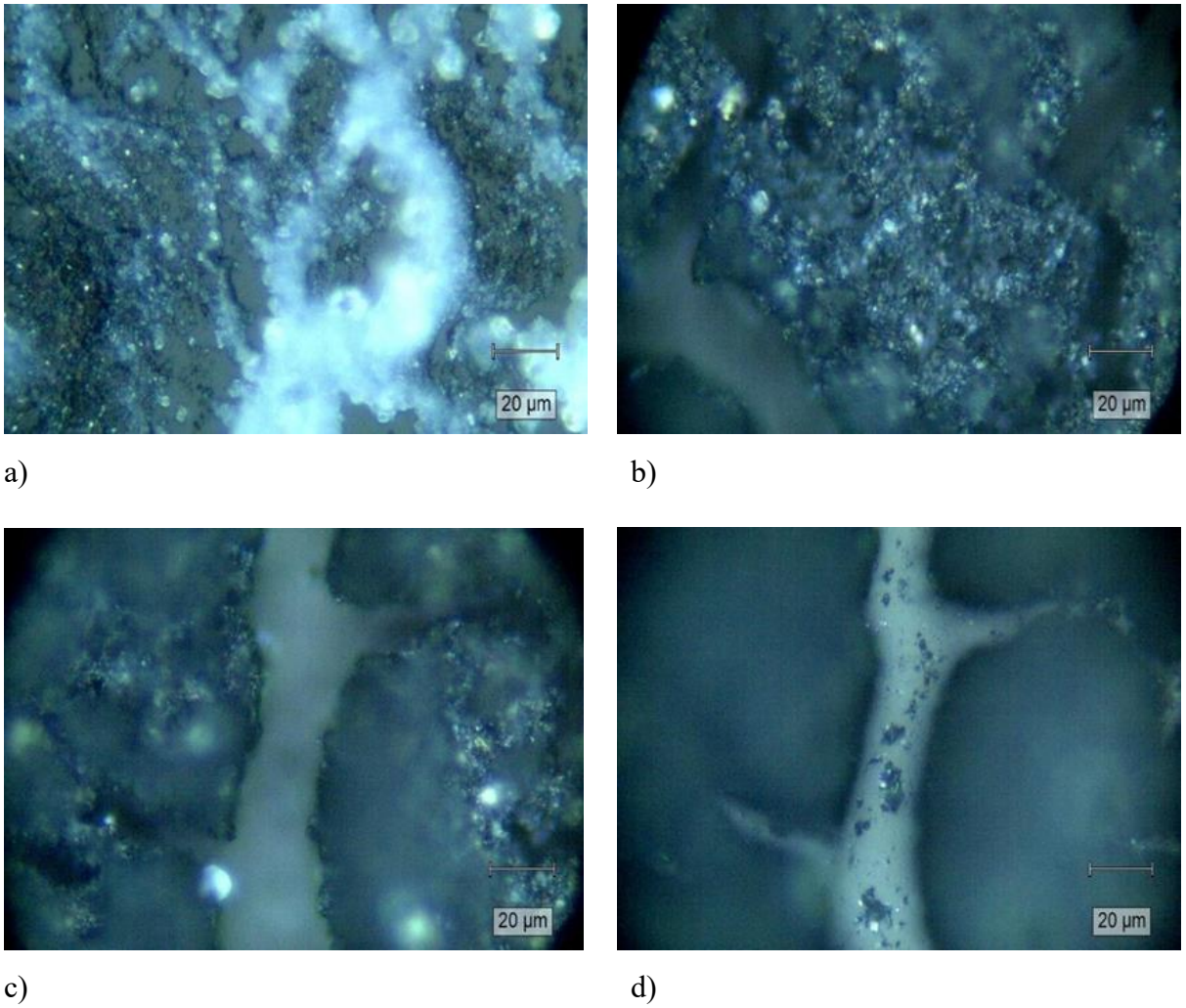

a) b)

c) d)

Figure 13. Raman Images of a) CeO_2 nanoparticles and b-d) CeO_2-RGO nanocomposites.

The XRD pattern of CeO_2 nanoparticles showed the diffracted peaks with high intensity were detected at 28.33, 32.95, 47.40 and 56.42 corresponds to 111, 200, 220 and 311 crystal planes as shown in figure 14. The diffracted peaks from XRD spectrum showed the cubic fluorite structure. The mean crystallite size of CeO_2 nanoparticles was 6.5 nm and it was determined by using the (FWHM) full width half maximum while using Scherrer's equation [53].

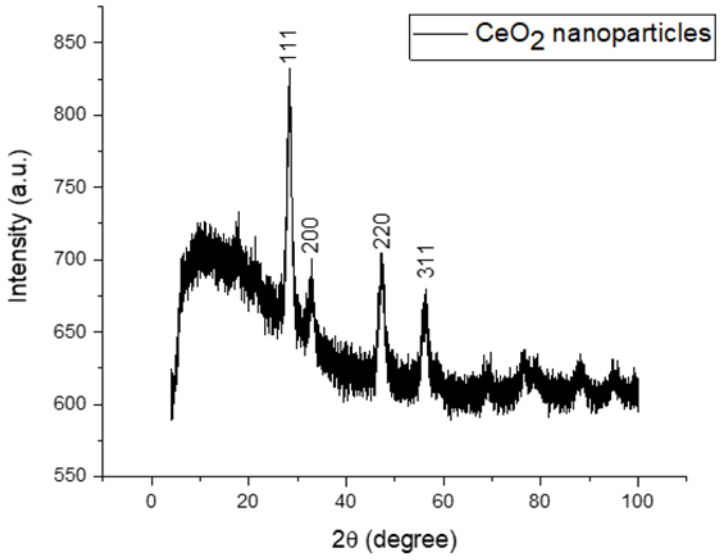

Figure 14. The XRD spectrum of (CeO_2) nanoparticles.

The XRD pattern of (CeO_2-RGO) nanocomposites showed the diffracted peaks with high intensity were detected at 28.49, 32.79, 47.23 and 56.42 corresponds to 111, 200, 220 and 311 crystal planes as shown in figure 15. The high intensity diffracted peaks in (CeO_2-RGO) nanocomposites are very similar to the CeO_2 nanoparticles. Which showed that CeO_2 nanoparticles anchored successfully on the RGO. The mean crystallite size for (CeO_2-RGO) nanocomposites was 11.8 nm and it was determined by using the (FWHM) full width half maximum while using Scherrer's equation. The presence of broad peak around 2θ=20 indicates the partial reduction of graphene oxide (GO) to reduced graphene oxide (RGO) [22].

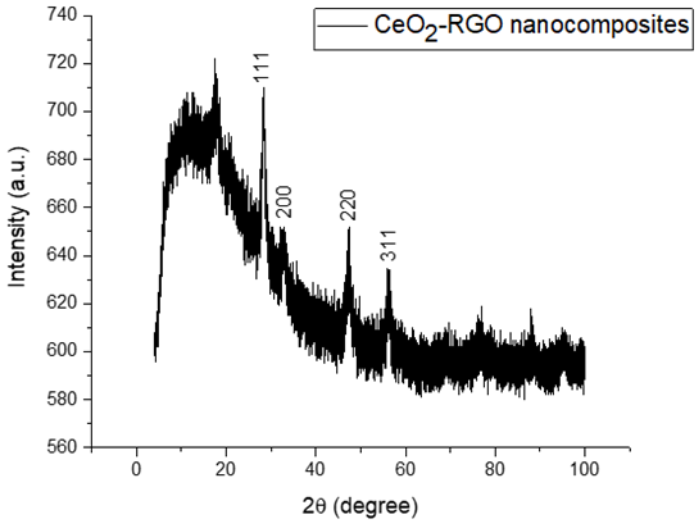

Figure 15. The XRD spectrum of (CeO_2-RGO) nanocomposites.

12. Electrochemical Measurements:

The cyclic voltammetry (CV) technique was used to analyse the electrochemical properties of CeO_2 nanoparticles and (CeO_2-RGO) nanocomposites. The three-electrode cell system was used for the electrochemical measurements is shown in figure 16.

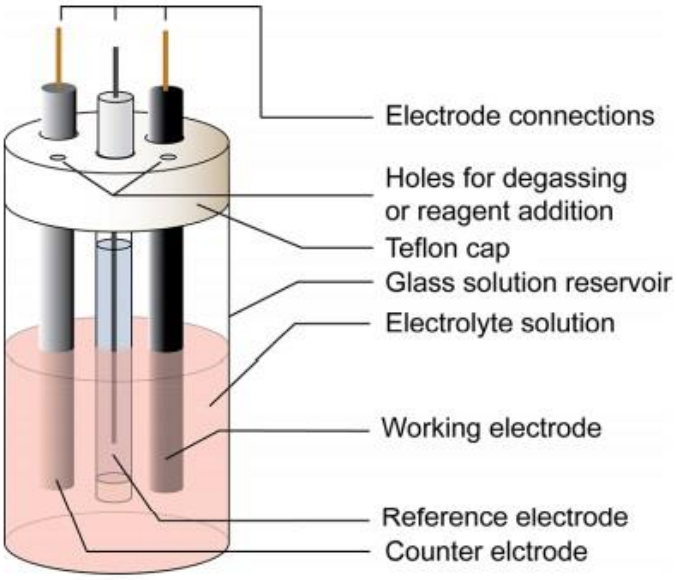

Figure 16. The electrochemical cell image [55].

The dried ceria (CeO_2) nanoparticles and (CeO_2-RGO) nanocomposites (1mg) were separately dispersed in ethanol (1ml) and sonicated for 30 minutes to acquire an even dispersion and then resulting suspension (2.5µl) was dropped on the surface of glassy carbon (GC) electrode and left it to get dry at room temperature. The oxygen reduction was carried out by using aprotic solvent. The three-electrode cell system was used, filled the cell with 5 ml of 0.1M tetrabutylammonium tetrafluoroborate in acetonitrile (dried) solution and bubbled the solution with N_2 gas for 30 minutes to remove the dissolved gases. After that attached the platinum (Pt) wire with counter electrode, silver wire coated with silver chloride layer (Ag/AgCl) with reference electrode and glassy carbon (GC) (cleaned) with working electrode, then used the Autolab Nova 2.1.4 software cyclic voltammetry measurement using a potentiostat. Measurement set up the starting point was zero volt, the first turning point was -2.1 volt and the second turning point was zero volt, run the three cycles with scan rate of 50mV/sec. After that bubbled the 0.1M tetrabutylammonium tetrafluoroborate in acetonitrile (dried) solution with O_2 gas for 30 minutes. Then repeated the measurements with coated (CeO_2-RGO) nanocomposites and then CeO_2 nanoparticles coated on glassy carbon (GC) electrode. Then compared the first scan of each bubbled with O_2 gas.

In Figure 17 the two oxygen reduction processes were observed in the O_2 saturated solution. The first reduction peak for ceria nanoparticles, (CeO_2-RGO) nanocomposites and bare glassy carbon (GC) electrode was quite similar with little position difference. The second reduction peak current observed was different with coated ceria nanoparticles at potential (-1.82) volt as compared to the (CeO_2-RGO) at potential (-1.83) volt and bare glassy carbon (GC) electrode was at potential (-1.92) volt. The oxidation peak observed was also similar with little position difference for the ceria nanoparticles, (CeO_2-RGO) and bare glassy carbon electrode. The peak separation between anodic and cathodic peak is large, for one electron reversible process it should be 59mV because of that process seems to be quasi reversible or irreversible. The electrocatalytic effect of ceria nanoparticles was observed in the reduction of oxygen.

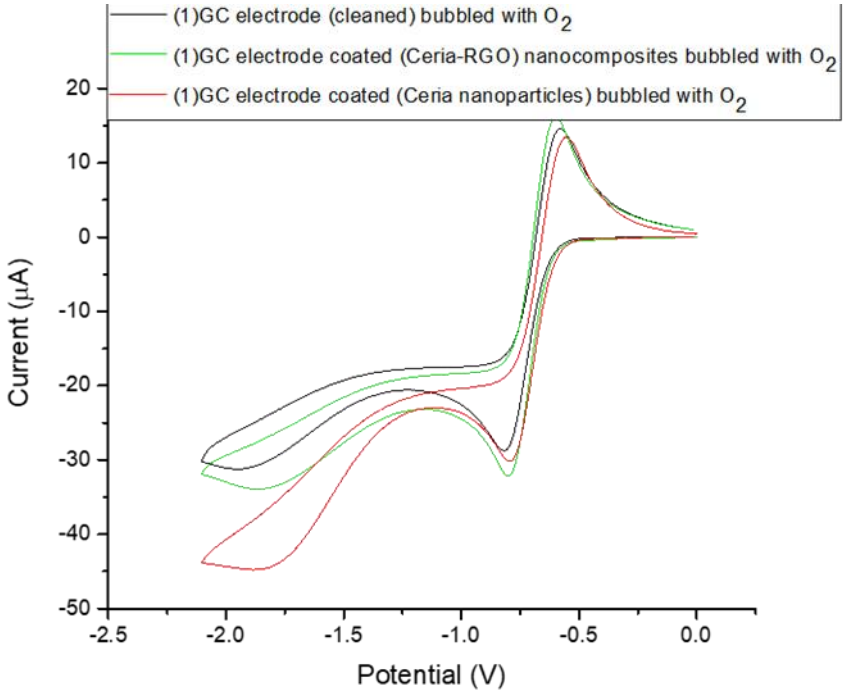

Figure 17. CV of GC electrode cleaned and coated with ceria nanoparticles and (Ceria-RGO) nanocomposites, (0.1M tetrabutylammonium tetrafluoroborate) in acetonitrile (dried) solution bubbled with O_2 gas.

The three-electrode cell system was used and filled the cell with 5ml of the 0.1M sodium sulphate (Na_2SO_4) solution in distilled water. Then bubbled the solution with N_2 gas for 30 minutes to remove the dissolved gases. After that attached the platinum (Pt) wire with counter electrode, silver wire coated with silver chloride layer (Ag/AgCl) with reference electrode and bare glassy carbon (GC) electrode with working electrode, then used the Autolab Nova 2.1.4 software cyclic voltammetry measurement using a potentiostat. Measurement set up the starting point was zero volt, the first turning point was -1.5 volt and the second turning point was zero volt, run the three cycles with scan rate of 50mV/sec. After that bubbled the 0.1M sodium sulphate (Na_2SO_4) in distilled water with O_2 gas for 30 minutes and repeated the experiment with coated (Ceria-RGO) nanocomposites on GC electrode. Then compared the first scan of bare GC electrode and coated with (Ceria-RGO) nanocomposites bubbled with oxygen (O_2) gas.

In Figure 18 the large reduction current peak at potential (-1.06) volt was observed as compared to the bare glassy carbon (GC) electrode which was observed at potential (-0.63) volt. There was no oxidation peak observed. The process seems to be irreversible. The catalytic effect of the (Ceria-RGO) nanocomposites was clearly observed. The (Ceria-RGO) nanocomposites

showed a synergistic effect. The electrocatalytic reduction of oxygen was carried out while using (Ceria-RGO) nanocomposites in neutral media [27,35].

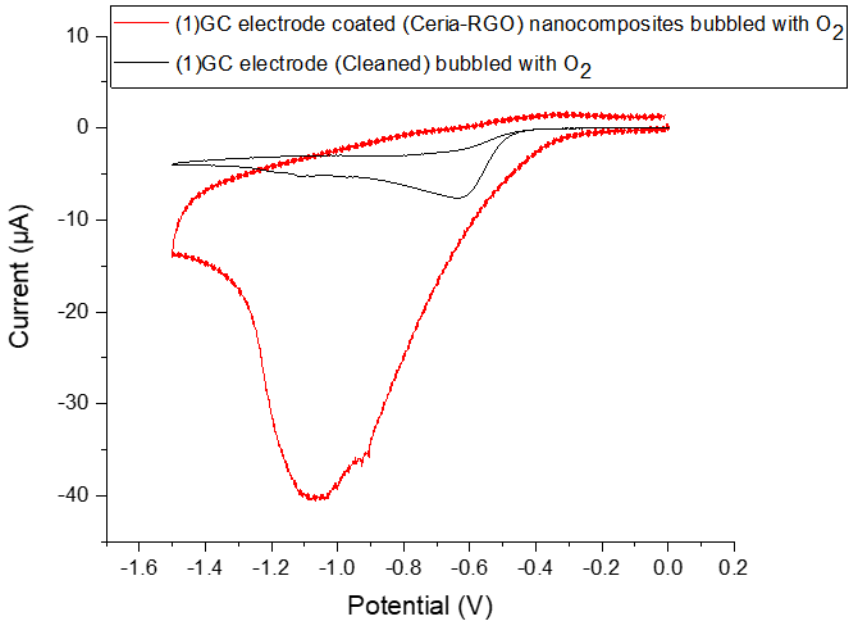

Figure 18. CV of GC electrode cleaned and coated with (Ceria-RGO) nanocomposites with scan rate 50mV/sec, (0.1M Na_2SO_4) aqueous solution bubbled with O_2 gas.

The oxygen reduction was observed in the aqueous solutions with different scan rates (5mV/sec and 20mV/sec). The three-electrode cell system was used and filled the cell with 5ml of the 0.1M sodium sulphate (Na_2SO_4) solution in distilled water. Then bubbled the solution with N_2 gas for 30 minutes to remove the dissolved gases. After that attached the platinum (Pt) wire with counter electrode, silver wire coated with silver chloride layer (Ag/AgCl) with reference electrode and coated (Ceria-RGO) glassy carbon (GC) electrode with working electrode, then used the Autolab Nova 2.1.4 software cyclic voltammetry measurement using a potentiostat. Measurement set up the starting point was zero volt, the first turning point was -1.5 volt and the second turning point was 0.8 volt, run the three cycles with scan rate of 5mV/sec and then with 20mV/sec. After that bubbled the 0.1M sodium sulphate (Na_2SO_4) in distilled water with O_2 gas for 30 minutes and run the three cycles with scan rate of 5mV/sec and 20mV/sec. Then compared the first scan of N_2 and O_2 saturated solution coated with (Ceria-RGO) nanocomposites.

In Figure 19 the clear high reduction current peak at potential (-0.98) volt was observed with coated (Ceria-RGO) nanocomposites on GC electrode in the O_2 saturated solution as compared to N_2 bubbled solution coated with (Ceria-RGO) nanocomposites on the surface of glassy carbon (GC). The electrocatalytic activity of (Ceria-RGO) nanocomposites was observed in the reduction of oxygen.

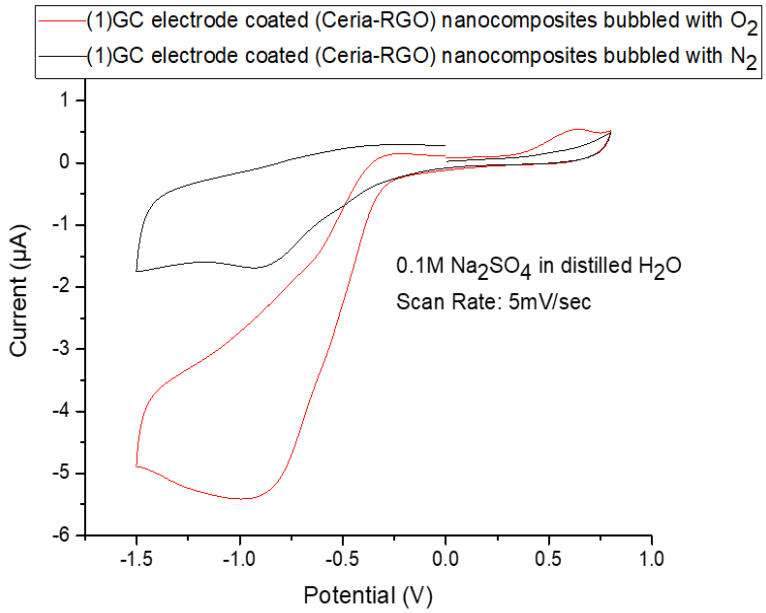

Figure 19. CV of GC electrode coated with (Ceria-RGO) nanocomposites with scan rate 5mV/sec, (0.1M Na_2SO_4) aqueous solution bubbled with N_2 and O_2 gas.

In Figure 20 the high reduction current peak at potential (-0.91) volt was observed with coated (Ceria-RGO) nanocomposites on GC electrode in the O_2 saturated solution as compared to N_2 bubbled solution coated with (Ceria-RGO) nanocomposites on the surface of glassy carbon (GC). The clear electrocatalytic effect of (Ceria-RGO) nanocomposites in the reduction of oxygen was observed.

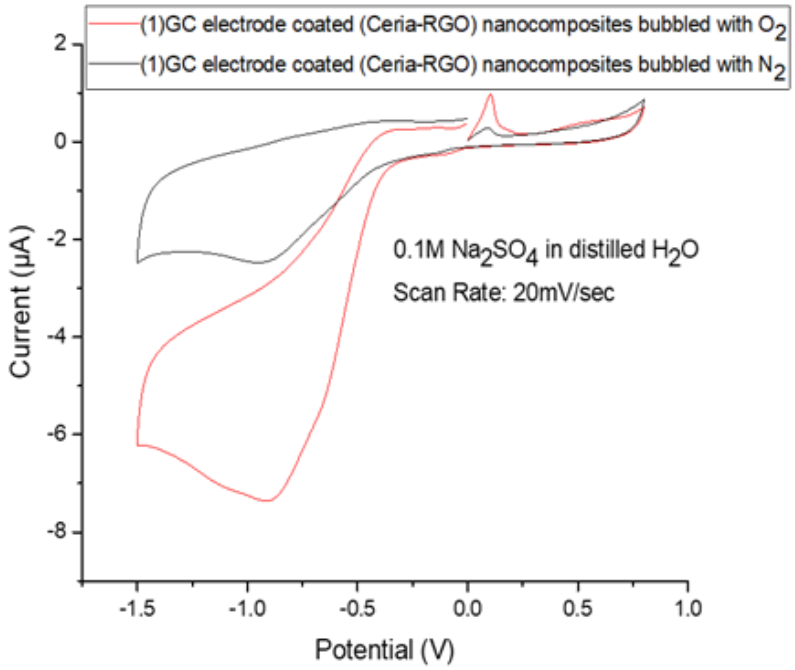

Figure 20. CV of GC electrode coated with (Ceria-RGO) nanocomposites with scan rate 20mV/sec, (0.1M Na_2SO_4) aqueous solution bubbled with N_2 and O_2 gas.

Figure 21 shows CVs of GC electrode coated with (Ceria-RGO) nanocomposites with scan rate 5, 10, 20, 50, 100 and 200 mV/sec, (0.1M Na_2SO_4) in aqueous solution bubbled with O_2 gas. The reduction peak current increases with increase in the scan rates. The reduction peak position is also shifted with the scan rate, this shift in the potential which indicates the more active sites present in the (Ceria-RGO) nanocomposites. The Randles-Sevick plot between the cathodic current and square root of scan rate does not seem to be linear as shown in figure 22. In Randles-Sevick plot it is difficult to accurately assign the peak current because of the two overlapping reactions. The reduction process seems to be irreversible.

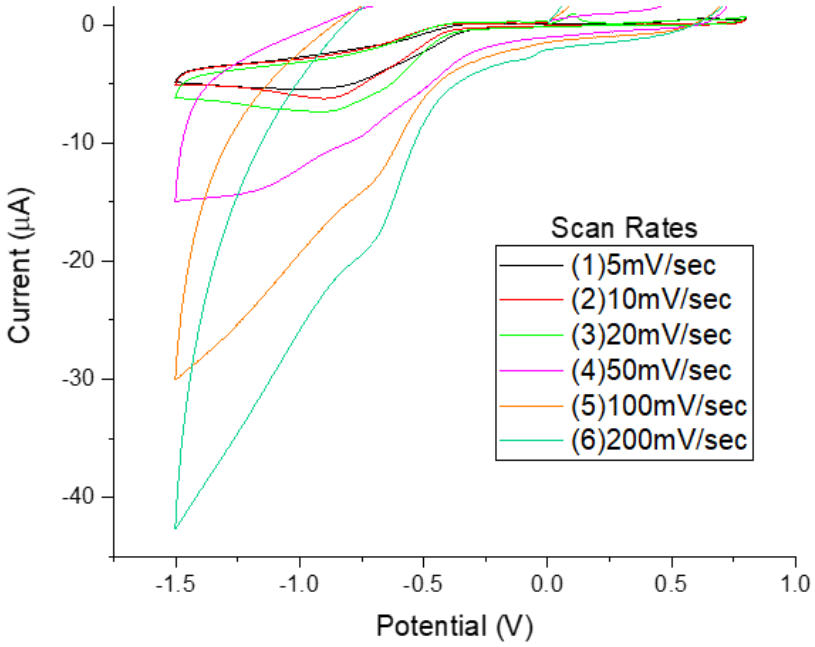

Figure 21. shows CVs of GC electrode coated with (Ceria-RGO) nanocomposites with scan rate 5, 10, 20, 50, 100 and 200 mV/sec (0.1M Na_2SO_4) in aqueous solution bubbled with O_2 gas.

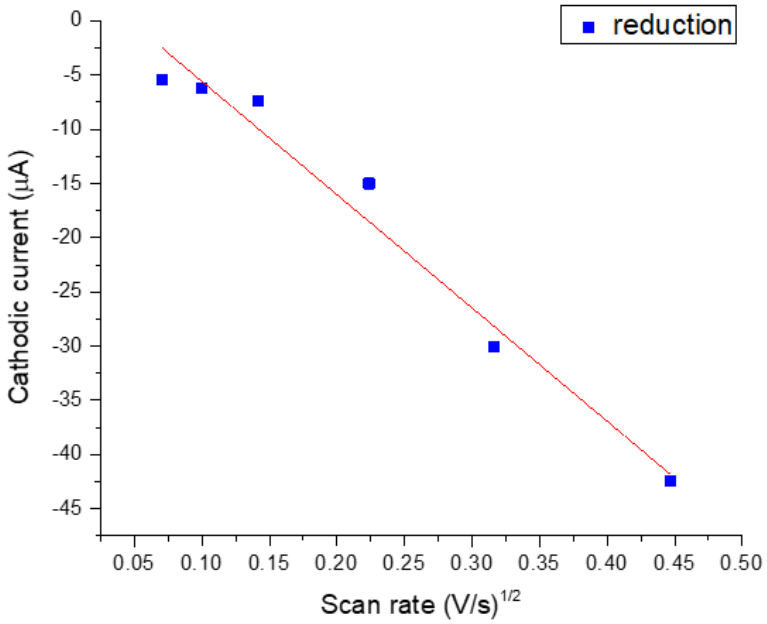

Figure 22. Randles-Sevick plot between square root of scan rates (5, 10, 20, 50, 100 and 200) mV/sec and the corresponding cathodic current.

Scan Rate(mV/sec)	Scan Rate(V/sec)	SQRT(Scan RateV/sec)	Cathodic Current(μA)
5	0.005	0.0707	-5.42
10	0.01	0.1	-6.24
20	0.02	0.1414	-7.39
50	0.05	0.2236	-15
100	0.1	0.3162	-30.09
200	0.2	0.4472	-42.48

Table 1. Square root of scan rates 5, 10, 20, 50, 100 and 200 mV/sec and corresponding cathodic current.

The catalytic effect of (Ceria-RGO) nanocomposites was also observed while using gold (Au) as working electrode in aprotic solvent. The three-electrode cell system was used, filled the cell with 5ml of the 0.1M tetrabutylammonium tetrafluoroborate in acetonitrile (dried) solution and bubbled the solution with N_2 gas for 30 minutes to remove the dissolved gases. After that attached the platinum (Pt) wire with counter electrode, silver wire coated with silver chloride layer (Ag/AgCl) with reference electrode and gold (Au) electrode (cleaned) with working electrode, then used the Autolab Nova 2.1.4 software cyclic voltammetry measurement using a potentiostat. Measurement set up the starting point was zero volt, the first turning point was -2.1 volt and the second turning point was 0,8 volt, run the three cycles with scan rate of 50mV/sec. After that bubbled the 0.1M tetrabutylammonium tetrafluoroborate in acetonitrile (dried) solution with O_2 gas for 30 minutes. Then repeated the same measurements with GC electrode coated with (Ceria-RGO) nanocomposites and compared the first scan of each.

In Figure 23 the two oxygen reduction processes were observed with gold (Au) electrode coated with (Ceria-RGO) nanocomposites in O_2 saturated solution. The first reduction peak at potential (-0.73) volt started early as compared to the bare gold electrode which was at potential (-1.0) volt. The clear electrocatalytic effect of the (Ceria-RGO) nanocomposites was observed.

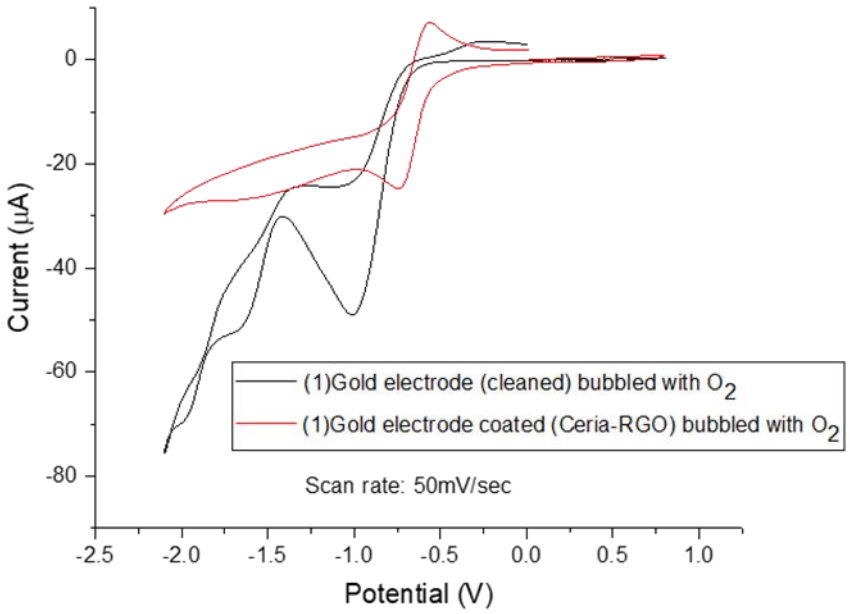

Figure 23. CV of Gold electrode cleaned and coated with (Ceria-RGO) nanocomposites with scan rate 50mV/sec, 0.1M tetrabutylammonium tetrafluoroborate in acetonitrile (dried) solution bubbled with O_2 gas.

The oxygen reduction was also observed in the aqueous solution with different scan rates (5mV/sec and 50mV/sec), while using coated (CeO_2-RGO) on gold (Au) electrode. The three-electrode cell system was used and filled the cell with 5ml of the 0.1M sodium sulphate (Na_2SO_4) solution in distilled water. Then bubbled the solution with N_2 gas for 30 minutes to remove the dissolved gases. After that attached the platinum (Pt) wire with counter electrode, silver wire coated with silver chloride layer (Ag/AgCl) with reference electrode and coated (Ceria-RGO) gold (Au) electrode with working electrode, then used the Autolab Nova 2.1.4 software cyclic voltammetry measurement using a potentiostat. Measurement set up the starting point was zero volts, the first turning point was -1.5 volt and the second turning point was 0.8 volt, run the three cycles first with scan rate of 5mV/sec and then with 50mV/sec. After that bubbled the 0.1M sodium sulphate (Na_2SO_4) in distilled water with O_2 gas for 30 minutes and run the three cycles with scan rate of 5mV/sec and 50mV/sec. Then compared the first cycle of N_2 and O_2 saturated solution coated with (Ceria-RGO) nanocomposites.

In Figure 24 there was no reduction peak observed in the N_2 bubbled solution coated with (Ceria-RGO) nanocomposites. The two reduction processes were noticed in the O_2 saturated solution. The first reduction peak was observed at potential (-0.46) volt and second reduction

peak was at (-1.05) volt in the O_2 saturated solution coated with (Ceria-RGO) nanocomposites on the surface of gold (Au) electrode. There was no oxidation peak was observed, and the process seems to be irreversible. The clear electrocatalytic effect of (Ceria-RGO) nanocomposites was observed in the reduction of oxygen.

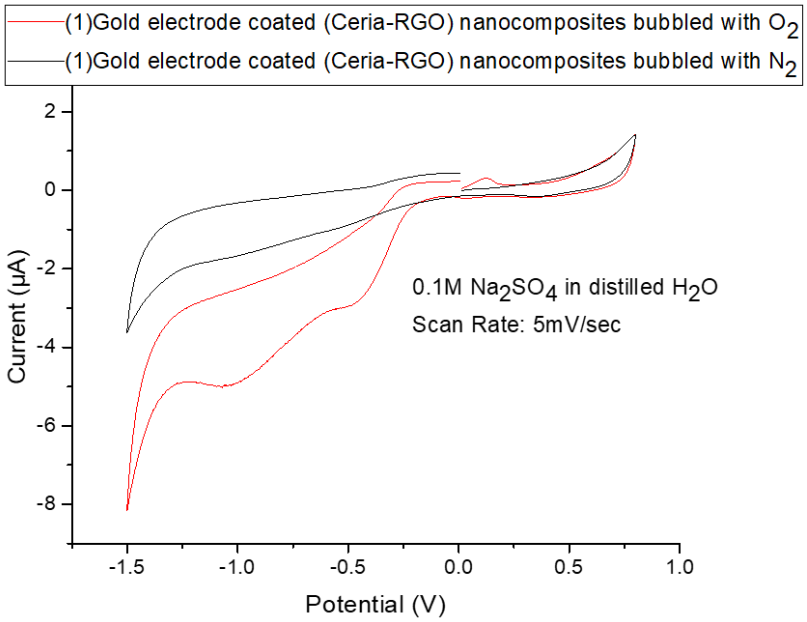

Figure 24. CV of Gold electrode coated with (Ceria-RGO) nanocomposites with scan rate 5mV/sec, (0.1M Na_2SO_4) aqueous solution bubbled with N_2 and O_2 gas.

In Figure 25 The two reduction processes were noticed in the O_2 saturated solution. The first reduction peak observed at potential (-0.45) volt and second high reduction current peak was at (-1.11) volt in the O_2 saturated solution coated with (Ceria-RGO) nanocomposites on the surface of gold (Au) electrode. The process seems to be irreversible. The clear electrocatalytic effect of (Ceria-RGO) nanocomposites was observed in the reduction of oxygen.

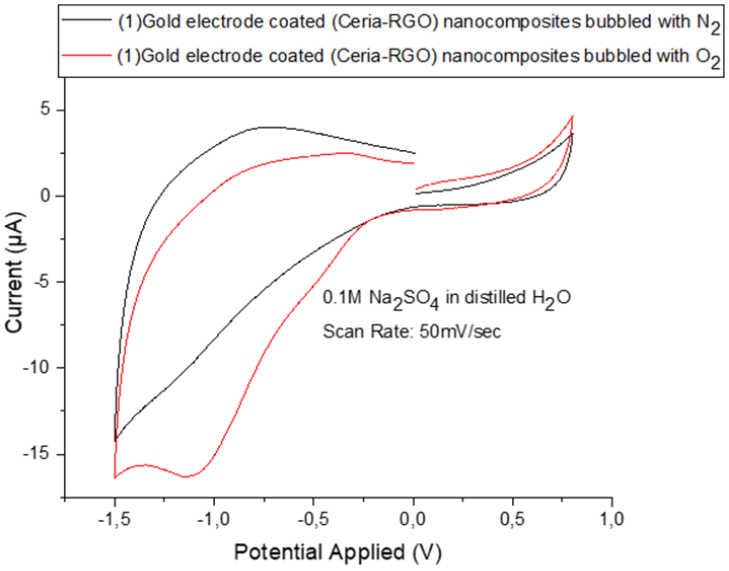

Figure 25. CV of Gold electrode coated with (Ceria-RGO) nanocomposites with scan rate 50mV/sec, (0.1M Na_2SO_4) aqueous solution bubbled with N_2 and O_2 gas.

The electrocatalytic reduction of *para*-nitrophenol was performed in the aprotic solvent (dried acetonitrile). The three-electrode cell system was used, filled 5ml of (0.1M tetrabutylammonium tetrafluoroborate + 0.05M *para*-nitrophenol) solution and bubbled the solution with N_2 gas for 30 minutes to remove the dissolved gases. After that attached the platinum (Pt) wire with counter electrode, silver wire coated with silver chloride layer (Ag/AgCl) with reference electrode and glassy carbon (GC) (cleaned) with working electrode, then used the Nova 2.1.4 software cyclic voltammetry measurement using a potentiostat. Measurement set up the starting point was zero volt, the first turning point was -2.1 volt and the second turning point was 0.8 volt, run the three cycles with scan rate of 50mV/sec and then 100mV/sec. After that bubbled the solution with O_2 gas for 30 minutes and run the three cycles with scan rate of 50mV/sec and then 100mV/sec. Then repeated the measurements with (CeO_2-RGO) nanocomposites coated on GC electrode and compared the first scan of glassy carbon (GC) cleaned and coated with (CeO_2-RGO).

In Figure 26 and 27 the reduction and oxidation peaks were almost at same position with (Ceria-RGO) nanocomposites coated on glassy carbon (GC) and cleaned glassy carbon (GC) electrode. There was no shift in the potential was observed so it can be concluded that electrochemical reduction of *para*-nitrophenol was not successful while using (Ceria-RGO) nanocomposites coated on glassy carbon (GC) electrode in aprotic solvent.

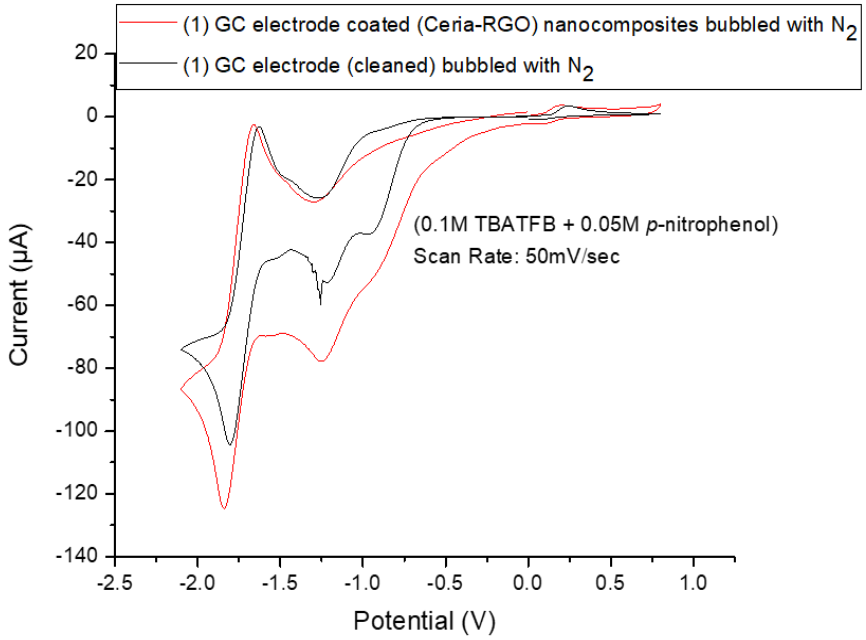

Figure 26. CVs of GC electrode cleaned and coated with (Ceria-RGO) nanocomposites with scan rate 50mV/sec, (0.1M tetrabutylammonium tetrafluoroborate + 0.05M *p*-nitrophenol) solution in dried acetonitrile bubbled with N_2 gas.

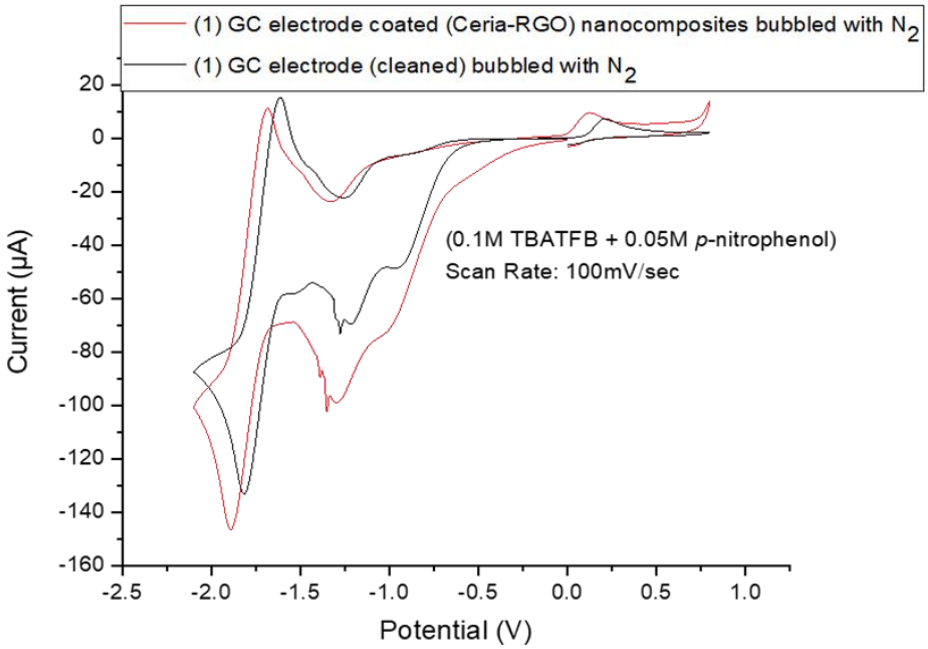

Figure 27. CV of GC electrode cleaned and coated with (Ceria-RGO) nanocomposites with scan rate 100mV/sec, (0.1M tetrabutylammonium tetrafluoroborate + 0.05M *p*-nitrophenol) solution in dried acetonitrile bubbled with N_2 gas.

The electrocatalytic reduction of *p*-nitrophenol was also carried out in aqueous solution. The three-electrode cell system was used and filled the cell with 5ml of (0.5M KOH + 0.05M *p*-nitrophenol) solution and bubbled the solution with N_2 gas for 30 minutes to remove the dissolved gases. After that attached the platinum (Pt) wire with counter electrode, silver wire coated with silver chloride layer (Ag/AgCl) with reference electrode and glassy carbon (GC) (cleaned) with working electrode, then used the Autolab Nova 2.1.4 software cyclic voltammetry measurement using a potentiostat. Measurement set up the starting point was zero volt, the first turning point was -1.7 volt and the second turning point was 1.0 volt, run the three cycles with scan rate of 50mV/sec. Then repeated the measurements with coated (ceria + pyrrole) nanoparticles on the surface of GC electrode. After that compared the first scan of glassy carbon (GC) cleaned and coated with (ceria + pyrrole). The pyrrole was used as an additive to enhance the electrical conductivity.

In Figure 28 the large reduction current peak of *para*-nitrophenol was observed at potential (-0.89) volt with coated (ceria+pyrrole), which started early as compared to the bare glassy carbon (GC) electrode which was observed at potential (-0.86) volt. This shows the clear electrocatalytic activity of the ceria nanoparticles in the reduction of *para*-nitrophenol [52].

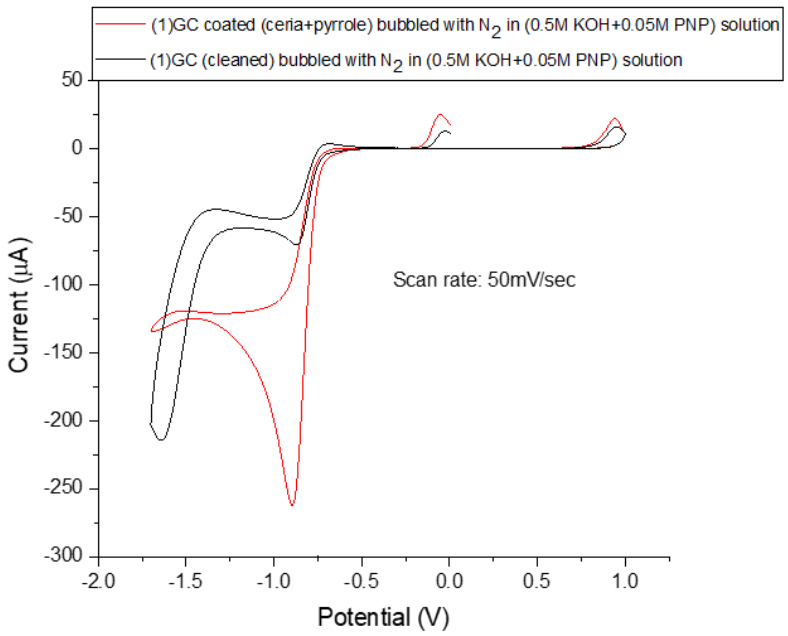

Figure 28 CVs of GC electrode cleaned and coated with (Ceria+pyrrole) nanoparticles with scan rate 50mV/sec, (0.5M KOH + 0.05M *p*-nitrophenol) solution bubbled with N_2 gas.

The electrocatalytic oxidation of methanol was performed in alkaline medium. The three-electrode cell system was used, filled the cell with 5ml of 0.5M sodium hydroxide (NaOH) solution and bubbled the solution with N_2 gas for 30 minutes to remove the dissolved gases. After that attached the platinum (Pt) wire with counter electrode, silver wire coated with silver chloride layer (Ag/AgCl) with reference electrode and glassy carbon (GC) coated with ceria nanoparticles with working electrode, then used the Autolab Nova 2.1.4 software cyclic voltammetry measurement using a potentiostat. Measurement set up the starting point was zero volt, the first turning point was zero volt and the second turning point was 1.0 volt, run the three cycles with scan rate of 50mV/sec. Then repeated the same measurement with glassy carbon (GC) coated with ceria nanoparticles in the presence of 0.5M methanol in 0.5M NaOH solution. After that compare, the first scans of both. In Figure 29 there is no response with glassy carbon (GC) electrode coated with ceria nanoparticles in the absence of methanol, whereas the high oxidation peak current was observed with (GC) coated with ceria nanoparticles in the presence of methanol in alkaline media. This showed clearly the electrocatalytic activity of ceria nanoparticles in the oxidation of methanol. The electrocatalytic oxidation of methanol was carried out with ceria nanoparticles in alkaline media [33,34].

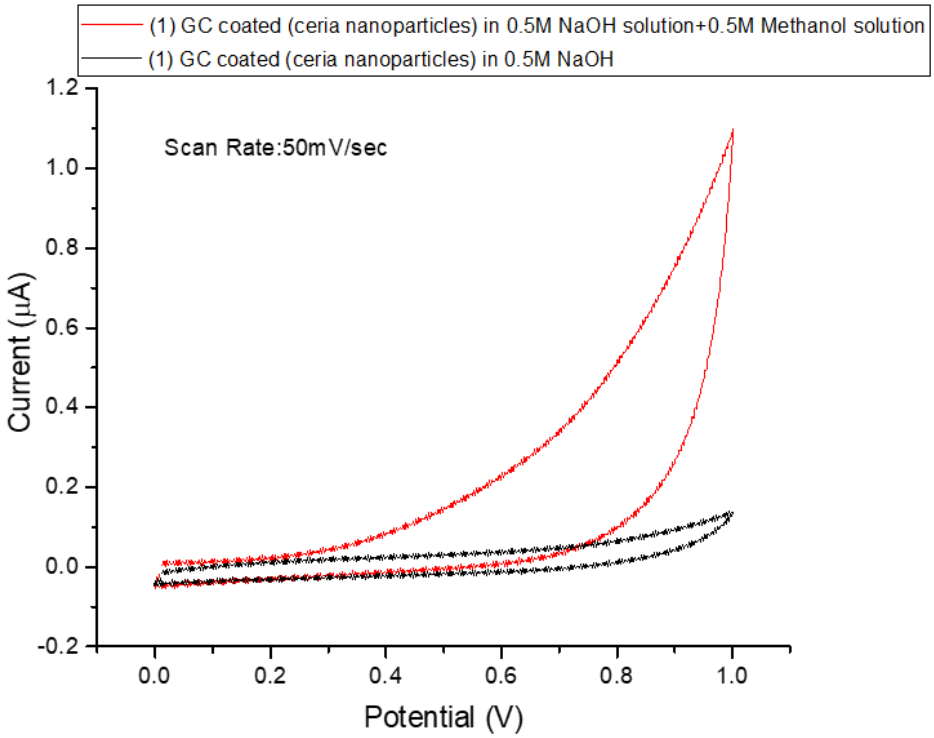

Figure 29. CV of GC electrode coated with ceria nanoparticles in 0.5M NaOH and 0.5M NaOH+0.5M methanol solution with scan rate of 50mV/sec.

The electrocatalytic reduction of oxygen was carried out. The three-electrode cell system was used, bubbled the 0.1M sodium sulphate (Na_2SO_4) in distilled water solution with N_2 gas for 30 minutes to remove the dissolved gases. After that attached the platinum (Pt) wire with counter electrode, silver wire coated with silver chloride layer (Ag/AgCl) with reference electrode and glassy carbon (GC) electrode coated with (Ceria-RGO) nanocomposites dipped in pyrrole solution (pH=2) with working electrode, then used the Autolab Nova 2.1.4 software cyclic voltammetry measurement using a potentiostat. Measurement set up the starting point was zero volts, the first turning point was -1.5V and the second turning point was 0.8 volt, run the three cycles with scan rate of 50mV/sec. After that bubbled the 0.1M sodium sulphate (Na_2SO_4) in distilled water with O_2 gas for 30 minutes. Then compared the first scan bubbled with N_2 and then O_2 gas.

In Figure 30 the high reduction current peak was observed around (-0.34) volt in the O_2 saturated solution coated with (Ceria-RGO/pyrrole) nanocomposites as compared to the N_2 bubbled solution coated with (Ceria-RGO/pyrrole) nanocomposites. The high oxidation peak current was also observed in both N_2 and O_2 saturated solutions with coated (CeO_2-RGO/pyrrole) nanocomposites on glassy carbon (GC) electrode which is because of the polypyrrole. The pyrrole was used as an additive to promote the oxygen reduction and to enhance the ORR performance [32].

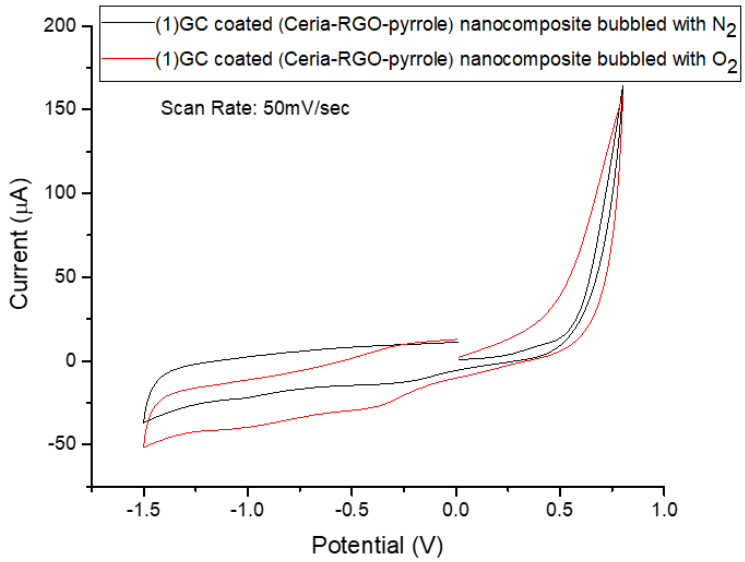

Figure 30. CV of GC electrode coated with (Ceria-RGO/pyrrole) nanocomposites in 0.1M Na_2SO_4 aqueous solution bubbled with N_2 and O_2 gas with scan rate of 50mV/sec.

In Figure 31 the capacitive behaviour of (CeO_2-RGO) nanocomposites was examined. The three-electrode cell system was used, bubbled the 0.1M sodium sulphate (Na_2SO_4) in distilled water solution with N_2 gas for 30 minutes to remove the dissolved gases. After that attached the platinum (Pt) wire with counter electrode, silver wire coated with silver chloride layer (Ag/AgCl) with reference electrode and glassy carbon (GC) electrode coated with (CeO_2-RGO) nanocomposites dipped in pyrrole solution (pH=2) with working electrode, then used the Autolab Nova 2.1.4 software cyclic voltammetry measurement using a potentiostat. The measurement set up starting point was zero volt, the first turning point was -1.0 volt and the second turning point was -0.2 volt, run the three cycles with scan rate of 20, 50, 100mV/sec and make the comparison of first scan of each. The shapes of the peaks are not an ideal rectangular [58] which showed its pseudo capacitance behaviour. The capacitance of (CeO_2-RGO) nanocomposites was calculated as (1.17×10^{-3}, 1.11×10^{-3} and 1.04×10^{-3}) F/cm^2 at the scan rates (20, 50 and 100) mV/sec, respectively. The calculated capacitance value decreases with the increase in scan rates as shown in Table 2.

Dezfuli A.S. et al. used the sonochemical method for the formation of (CeO_2-RGO) nanocomposites and the specific capacitance measured was 185 F g^{-1} at 2.0 A g^{-1}[41].

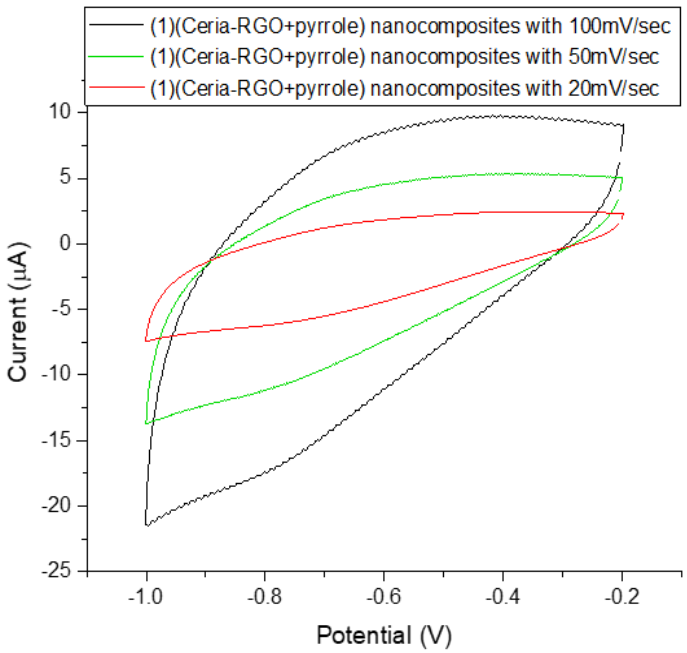

Figure 31. CVs of GC electrode coated with (Ceria-RGO/pyrrole) nanocomposites with scan rates (20, 50 and 100) mV/sec, in 0.1 M Na_2SO_4 solution bubbled with N_2 gas.

Scan Rate(mV/sec)	Scan Rate(V/sec)	Capacitance(F/cm^2)
20	0.02	1.17E-03
50	0.05	1.11E-03
100	0.1	1.04E-03

Table 2. The Scan rates 20, 50 and 100 mV/sec and corresponding capacitance.

The electrocatalytic reduction of oxygen was also observed by using rotating ring disc electrode (RRDE) technique. The two working electrodes were used, glassy carbon (disk electrode) and platinum (ring electrode), silver wire coated with silver chloride layer (Ag/AgCl) as a reference and platinum (Pt) wire as a counter electrode. Figures 32 and 33 showed the RRDE voltammograms recorded with bare and coated with (CeO_2-RGO) nanocomposite on RRDE electrode with scan rate 50mV/sec in 0.1M potassium hydroxide (KOH) solution saturated with oxygen (O_2) gas with different rotating rates. When the rotating rates are increased the limiting current also increased. The RRDE voltammograms showed that the anodic and cathodic current increased with increased rotating rates and the comparison between the bare RRDE electrode and coated with (CeO_2-RGO) nanocomposites on the surface of RRDE electrode showed that the two reduction and oxidation processes are involved in the electrocatalytic reduction of oxygen, and the processes started early with the coated (CeO_2-RGO) nanocomposites on RRDE electrode, as compared to the bare RRDE electrode. The catalytic effect of the (CeO_2-RGO) nanocomposites was observed by using this hydrodynamic technique.

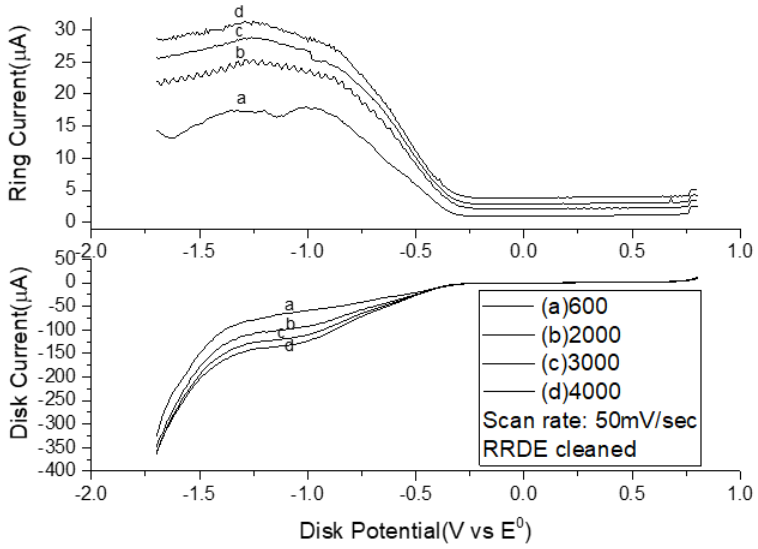

Figure 32. Voltammogram recorded with 600, 2000, 3000 and 4000 rpm with scan rate 50mV/sec, with cleaned RRDE electrode in 0.1M KOH solution.

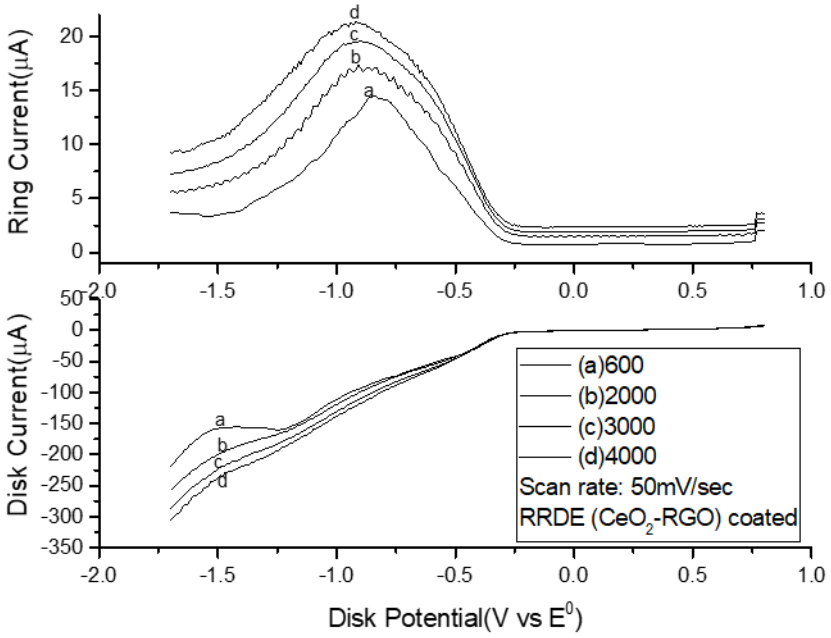

Figure 33. Voltammogram recorded with 600, 2000, 3000 and 4000 rpm with scan rate 50mV/sec, with coated (CeO_2-RGO) RRDE electrode in 0.1M KOH solution.

13. Conclusion:

The aim of the study was to synthesize and investigate the electrochemical properties of the ceria (CeO_2) nanoparticles and ceria-reduced graphene oxide (CeO_2-RGO) nanocomposites. The characterization techniques such as UV-visible, FTIR, Raman and XRD were used to confirm the successful formation of ceria (CeO_2) nanoparticles and ceria-reduced graphene oxide (CeO_2-RGO) nanocomposites. The XRD pattern of the ceria (CeO_2) nanoparticles shows structure of cubic fluorite for the ceria. The high intensity diffracted peaks in XRD pattern of (CeO_2-RGO) nanocomposites are very similar to the (CeO_2) nanoparticles. This showed that ceria (CeO_2) nanoparticles anchored successfully on the reduced graphene oxide (RGO). The cyclic voltammetry (CV) and rotating ring disc electrode (RRDE) techniques were used to perform electrochemical measurements. The electrocatalytic reduction of oxygen was successfully carried out with (CeO_2-RGO) nanocomposites coated on glassy carbon (GC) and gold (Au) electrodes in the protic and aprotic solvents. The two reduction processes were observed in the electrocatalytic reduction of oxygen. The oxygen reduction processes seem to be irreversible. The (CeO_2-RGO) nanocomposites is an effective catalyst and has high performance for oxygen reduction reaction (ORR) as compared to the ceria nanoparticles

because of the synergistic effect of exceptional reduced graphene oxide (RGO) electronic conductivity and oxygen vacancies present in ceria (CeO_2) nanoparticles. The reduced graphene oxide (RGO) improves the transfer of electrons, and the ceria (CeO_2) nanoparticles play as an electron facilitator. The electrocatalytic effect of oxygen reduction is most probably because of labile oxygen vacancies that are formed on the surface of ceria (CeO_2) nanoparticles. Oxygen reduction reaction (ORR) is very essential reaction in the energy converting systems for example in fuel cells. The (CeO_2-RGO) nanocomposite can be used in metal air batteries and fuel cells as a bifunctional electrocatalyst. The high oxidation peak current was observed for electrocatalytic oxidation of methanol in alkaline media with ceria (CeO_2) nanoparticles. The ceria (CeO_2) nanoparticles showed the electrocatalytic activity in the oxidation of methanol and further the ceria (CeO_2) nanoparticles can be appropriate material for direct methanol fuel cells (DMFCs). The capacitive behaviour of (CeO_2-RGO) nanocomposites was examined. The shapes of the peaks are not an ideal rectangular which showed its pseudo capacitance behaviour. The electrochemical measurements showed the (CeO_2-RGO) nanocomposites have capacitance of (1.17×10^{-3}, 1.11×10^{-3} and 1.04×10^{-3}) F/cm^2 at the scan rates (20, 50 and 100) mV/sec respectively because of the reduced graphene oxide (RGO) electrical conductivity and the ceria nanoparticles pseudo capacitance. The (CeO_2-RGO) nanocomposites can be used in the energy storage devices such as supercapacitors because of their electrochemical properties. The electrocatalytic reduction of *para*-nitrophenol (which is a toxic compound) was successfully carried out in aqueous solution with ceria (CeO_2) nanoparticles. The large reduction current peak of *para*-nitrophenol was observed at negative potential (-0.89) volt with coated ceria (CeO_2) nanoparticles on the glassy carbon (GC) electrode and the polypyrrole a conducting polymer was used to increase the conductivity. The (CeO_2-RGO) nanocomposites can induce synergistic effect to enhance the electrocatalytic activity. The potential applications of (CeO_2-RGO) nanocomposites are that they can be used as inexpensive catalyst in fuel cells and furthermore they can be examined for the electrocatalytic reduction of carbon dioxide (CO_2).

14. References:

1. Schelter, E. *Nature Chem.* **2013**, 5, 348.

2. Bouzigues, C.; Gacoin, T.; Alexandrou, A. *ACS Nano.* **2011**, 5, 8488-8505.

3. Younis, A.; Chu, D.; Li, S. Cerium oxide nanostructures, and their applications. **2016**, DOI: 10.5772/65937.

4. Reni, M. L.; Nesaraj, A. S. *Mater. Res. Innov.* **2020,** 25, 5, 276-286.

5. Reed, K.; Cormack, A.; Kulkarni, A.; et al. *Environ. Sci. Nano*, **2014,** 1, 390-405.

6. Molinari, M.; Parker, S. C.; Sayle, D. C.; Islam, M. S. *J. Phys. Chem. C* **2012**, 116, 7073-7082.

7. Dhall, A.; Self, W. *Antioxidants*, **2018**, 7, 97.

8. Sun, C.; Li, H.; Chen, L. *Energy Environ. Sci.* **2012**, 5, 8475.

9. Malavasi, L.; Fisher, C. A. J.; Islam, M. S. *Chem. Soc. Rev.* **2010**, 39, 4370-4387.

10. M. Nolan et al. *Solid-State Ionics*, **2006**, 177, 3069–3074.

11. Wang, Z. L.; Feng, X. D. *J. Phys. Chem. B* **2003**, 107, 13563-13566.

12. Campbell, C. T.; Peden, C. H. F. *Science*, **2005**, 309, 713-714.

13. Li, J.; Zhang, Z.; Tian, Z.; et al. *J. Mater. Chem. A* **2014**, 2, 16459.

14. Hailstone, R. K.; DiFrancesco, A. G.; Leong, J. G.; et al. *J. Phys. Chem. C* **2009**, 113, 15155-15159.

15. Deshpande, S. et al. App. Phys. Lett. **2005**, 87, 133113.

16. Ambrosi, A.; Bonanni, A.; Sofer, Z. K.; et al. *J. Chem. Eur.* **2011**, 17, 10763-10770.

17. Laval, A.T. *Biosens. Bioelectron.* **2019**, 141, 111384.

18. Pei, S.; Cheng, H.M. *Carbon*. **2012**, 50, 3210-3228.

19. Joung, D.; Singh, V.; Park, S.; et al. *J. Phys. Chem. C*, **2011**, 115, 24494-24500.

20. Griggs, C. S.; Medina, V. **2016** https://doi.org/10.1036/1097-8542. YB150695 2016

21. Srivastava, M.; Das, A. K.; Khanra, P.; et al. *J. Mater. Chem. A* **2013**, 1, 9792-9801.

22. Dezfuli, A.S.; et al. *J. Mater. Chem. B* **2015**, 3, 2362-2370.

23. Rajesh, U. C.; Wang, J.; Prescott, S.; et al. *ACS Sustainable Chem. & Eng.* **2015,** 3, 1, 9-18.

24. Park, S. H.; Kim, H. K.; Roh, K. C.; et al. *Electron. Mater. Lett.* **2015**, 11, 282-287.

25. Leal, J. F.; Cruz, S. M. A.; Almeida, B. T. A.; et al. *Environ. Sci.: Water Res. Technol*. **2020**, 6, 1018-1027.

26. Kim, J. Y.; Kim, K. H.; Yoon, S. B.; et al. *Nanoscale.* **2013,** 5 (15), 6804-6811.

27. Sun, L.; Zhou, L.; Yang, C.; Yuan, Y. *Int. J. Hydrogen Energy* **2017**, 42, 15140-15148.

28. Zhang, J.; Song, C. *Springer,* **2008**, 89-134.

29. Bag, S.; Roy, K.; Gopinath, C. S.; Raj, C. R. *ACS Appl. Mater. Interf.* **2014**, 6, 2692-2699.

30. Chinchen, G. C.; Denny, P. J.; Parker, D. G.; et al. *Catal.* **1987**, 30, 333-338.

31. Chowdhury, S.; Lin, K. S. *J. Nanomaterials*, **2011**, 157690.

32. Soren, S.; et al. *Front Chem.* **2019**, 7, 403.

33. Kaur, B.; Srivastava, R.; Satpati, B. *ACS Catalysis*, **2016**, 6, 2654-2663.

34. Salarizadeh, P.; Askari, M. B.; Mohammadi, M.; Hooshyari, K. *J. of Phys. and Chem. of Solids*, **2020**, 142, 109442.

35. Parwaiz, S.; et al. *J. Phys. Chem. C* **2017**, 121, 20165-20176.

36. Chen, Z.; Waje, M.; Li, W.; Yan, Y. *Angew. Chem. Int.* **2007**, 46, 4060-4063.

37. Jiang, L.; Yao, M.; Liu, B.; Li, Q.; Liu, R.; Lv, H.; et al. *J. Phys. Chem. C* **2012**, 116, 11741-11745.

38. Jaiswal, N.; Tanwar, K.; Suman, R.; et al. *J. of Alloys and Compounds*, **2019,** 781, 984-1005.

39. Chueh, W., Hao, Y., Jung, W. et al. *Nature Mater*, **2012**, 11, 155-161.

40. Yu, A.; Chabot, V.; Zhang, J.; Electrochemical Supercapacitors for Energy Storage and Delivery *CRC Press* Ed.1, **2013**.

41. Dezfuli, A. S.; Ganjali,M. R.; Naderi, H. R.; Norouzi, P. *RSC Adv.* **2015**, 5, 46050-46058.

42. Deng, D., Chen, N., Xiao, X.; et al. *Ionics*, **2017**, 23, 121-129.

43. Wang, Y.; Guo, C. X.; Liu, J.; Chen, T.; Yang, H.; Li, C. M. *Dalton transactions*, **2011**, 40, 6388-6391.

44. Francke, R.; Schille, B.; Roemelt, M. *Chem. Rev.* **2018,** 118, 4631-4701.

45. Esrafilzadeh, D.; et al. *Nature Communications*, **2019**, 10, 865.

46. Gust, D.; Moore, T. A.; Moore, A. L. *Acc. of Chem. Res.* **2009**, 42, 1890-1898.

47. Primo, A.; et al. *J. Am. Chem. Soc.* **2011**, 133, 6930-6933.

48. Verma, R.; Samdarshi, S. K. *J. Phys. Chem. C* **2016**, 120, 22281-22290.

49. Ji, Z. Y.; Shen, X. P.; Li, M. Z.; et al. *Nanotechnology*, **2013**, 24, 115603.

50. Houcini, H. et al. *Int. J. of Envir. Anal. Chem.* **2020**, 100, 1566-1577.

51. Miah, A. T. et al. *Catal. Lett.* **2016**, 146, 291-303.

52. Wu, S.; Fan, S.; Tan, S.; et al. *RSC Adv*. **2018**, 8, 775-784.

53. Chelliah, M.; et al. *J. Appl. Sci.* **2012**, 12, 16, 1734-1737.

54. Kumar, S.; Kumar, A. *Materials Science and Engineering B* **2017**, 223, 98-108.

55. Elgrishi, N.; et al. *J. Chem. Educ.* **2018**, 95, 197-206.

56. Nerkar, D. M.; Jaware, S. E.; Padhye, G. G. *Inter. J. of Sci. and Res.***2016**, 5, 3, 106-111.

57. Cui, Z.; et al. *Langmuir* **2014**, 30, 46, 14086-14094.

58. Hashmi, S.A.; Latham, R.J.; Linford, R.G.; et al. *Ionics* **1997**, 3, 177-183.